

1 Variability in ~~grain-sediment particle size~~, mineralogy, and Fe mode of  
2 occurrence ~~of Fe in surface sediments of preferential~~across dust-source inland  
3 drainage basins: The case of the Lower Drâa Valley, ~~S~~-Morocco

4 Adolfo González-Romero<sup>1,2,3</sup>, Cristina González-Florez<sup>1,3</sup>, Agnesh Panta<sup>4</sup>, Jesús Yus-Díez<sup>2,a</sup>, Cristina Reche<sup>2</sup>,  
5 Patricia Córdoba<sup>2</sup>, Andres Alastuey<sup>2</sup>, Konrad Kandler<sup>4</sup>, Martina Klose<sup>5</sup>, Clarissa Baldo<sup>6</sup>, Roger N. Clark<sup>7</sup>,  
6 Zong Bo Shi<sup>8</sup>, Xavier Querol<sup>2</sup>, Carlos Pérez García-Pando<sup>1,9</sup>

7  
8 <sup>1</sup>Barcelona Supercomputing Center (BSC), Barcelona, Spain

9 <sup>2</sup>Spanish Research Council, Institute of Environmental Assessment and water Research (IDAEA-CSIC),  
10 Barcelona, Spain

11 <sup>3</sup>Polytechnical University of Catalonia (UPC), environmental engineering doctoral programme, Barcelona,  
12 Spain

13 <sup>4</sup>Institute of Applied Geosciences, Technical University Darmstadt, Darmstadt, Germany

14 <sup>5</sup>Karlsruhe Institute of Technology (KIT), Institute of Meteorology and Climate Research (IMK-TRO),  
15 Department Troposphere Research, Karlsruhe, Germany

16 <sup>6</sup>Université Paris Cité and Univ Paris Est Creteil, CNRS, LISA, 75013 Paris, France

17 <sup>7</sup>PSI Planetary Science Institute, Tucson, AZ, USA

18 <sup>8</sup>School of Geography Earth and Environmental Sciences, the University of Birmingham, Birmingham,  
19 United Kingdom

20 <sup>9</sup>Catalan Institution for Research and Advanced Studies (ICREA), Barcelona, Spain

21 <sup>a</sup>now at: Center for Atmospheric Research, University of Nova Gorica, Ajdovščina, Slovenia.

22  
23 **Corresponding author:**

24 Adolfo González-Romero, <agonzal3@bsc.es>

25 Xavier Querol Carceller, <xavier.querol@idaea.csic.es>

Con formato: Español (España)

26  
27  
28  
29  
30  
31  
32  
33  
34  
35  
36  
37  
38  
39  
40  
41  
42  
43  
44  
45  
46  
47  
48  
49  
50  
51  
52

53  
54  
55  
56  
57  
58  
59  
60  
61  
62  
63  
64  
65  
66  
67  
68  
69  
70  
71  
72  
73  
74  
75  
76  
77  
78  
79  
80  
81  
82  
83  
84  
85  
86  
87  
88  
89  
90  
91  
92  
93  
94  
95  
96  
97  
98  
99  
100

## Abstract

The effects of mineral dust emitted desert dust from arid and semiarid surfaces upon climate and ecosystems ~~is highly affected by~~ depends strongly on ~~depends~~ fundamentally on ~~their~~ particle size ~~particle -size~~ distribution (PSD) and size-resolved mineralogical ~~composition~~ ical composition. However, there is very limited quantitative knowledge on the particle size and composition of the parent ~~sediments along with their variability within dust source regions, particularly in dust emission hotspots. This article presents a relevant dataset of dust-emitting sediments from, not only a Saharan, dust hotspot but also its surroundings, which is important to better understand their respective impacts on climate and air quality, and also their interactions.~~ However, soil mineralogy atlases used for mineral-speciated dust modelling are highly uncertain as they are derived ~~extrapolating mineralogical analyses of soil samples that are particularly scarce in dust source regions. This extrapolation neglects the processes affecting the formation of different dust-emitting surface sediments, such as dunes, crusts, and paved sediments.~~ The Lower Drâa Valley, an inland drainage basin and dust hotspot region and preferential dust source located in ~~southern Morocco~~ the Moroccan Sahara, was chosen for a comprehensive analysis of sediment ~~grain size~~ particle -size and mineralogy. Different sediment types samples ( $n=42$ ) were collected, including paleo-sediments, paved surfaces, crusts, and dunes, and analysed for particle -size distribution (through PSD analysis of minimally and fully dispersed samples) and mineralogy, and X-ray diffraction mineralogical analysis of bulk samples. We also performed ~~Furthermore, Fe sequential wet extraction was carried out to characterize the modes of occurrence of Fe, including Fe in Fe (Fe mineralogy, including the contents of (oxyhydr)oxides, mainly from (goethite and hematite), which are key to dust radiative effects), the and poorly crystalline pool of Fe (readily exchangeable ionic Fe and Fe in nano-Fe-oxides), relevant to dust impacts upon ocean biogeochemistry), and structural Fe. Based on the results~~ Results yield we propose a conceptual model where both particle size and mineralogy are segregated by transport and deposition of sediments during runoff of water across the basin, and by the precipitation of salts, which causes a sedimentary fractionation. The proportions of coarser particles (substantially richer/enriched in quartz) is higher are more present in elevated areas in the high-lands, and while that of finer particles (rich in clay, carbonates, and Fe-oxides) is higher in the low-lands are present in depressed areas, where dust emission is maximized dust emission hotspots. There, w When water ponds and evaporates, secondary carbonates and salts precipitate, and the clays are enriched in readily exchangeable ionic Fe, due to sorption of dissolved Fe by illite. ~~Our~~ These results differ from currently available mineralogical ~~atlases~~ atlases and highlight the need for observationally-constrained global high-resolution mineralogical data for mineral-speciated dust modeling. The obtained dataset represents an important resource for future evaluation of surface mineralogy retrievals from spaceborne spectroscopy.

**Keywords:** ~~Aeolian, desert, sediments, rid regions, arid land, dust sources, desert dust, dust-emitting~~ mineralogy, iron, Morocco sediments formation model, dust modelling.

101  
102  
103  
104  
105  
106  
107  
108  
109

## 1. Introduction

110 Desert dust is atmospheric particulate matter (PM), mostly mineral in composition, emitted ~~into~~  
111 ~~the atmosphere~~ by wind erosion of arid and semi-arid surfaces. The global dust source regions  
112 include North Africa, the Middle East, Central Asia, Western Australia, South America, Southern  
113 Africa and Southern US-Northern Mexico. ~~These regions include most of the so-called dust~~  
114 ~~emission “hotspots”, defined as localized, persistent areas of intense dust production within an~~  
115 ~~overall landscape which generally does not emit dust (Gillette, 1999; Baddock et al., 2016). From~~  
116 ~~these regions~~, North Africa accounts for around 50 % of the global dust emissions, followed by  
117 Central Asia, the Middle East and East Asia (Kok et al., 2021). Dust storms arise when strong  
118 winds generate a large amount of dust particles that drastically reduce visibility nearby and are  
119 transported over distances of hundreds of kilometres (Prospero et al. 2002). During transport,  
120 dust perturbs the energy and water cycles by direct radiative forcing and influences cloud  
121 formation, precipitation and the associated indirect radiative forcing (Weaver et al., 2002). Dust  
122 transports nutrients across the planet affecting ocean productivity (Boyd et al., 2007), plant  
123 nutrient gain or loss (Sullivan et al., 2007, [Doronzo et al., 2016](#), [Alshemmari et al., 2013](#), [Al-](#)  
124 [Dousari et al., 2020](#)), and glacier mass budgets (Goudie & Middleton, 2006). Dust can also  
125 directly affect human health by inhalation or by favouring the propagation of diseases (Goudie  
126 & Middleton, 2006, De Longeville et al., 2010; Karanasiou et al., 2012; Pérez García-Pando et al.,  
127 2014, [Al-Dousari et al., 2018](#)). It can reduce renewable solar energy output due to attenuation  
128 of solar radiation and soiling of solar panels ([Al-Dousari et al., 2019](#); Monteiro et al., 2022),  
129 create poor visibility on roads increasing the risk of traffic accidents (Middleton, 2017) and cause  
130 disturbances in airport operations and air traffic (Monteiro et al., 2022).

131 ~~(), and photovoltaic energy efficiency ()),~~

132 Dust is emitted mostly from arid inland drainage basins (~~Dubief, 1977~~; Prospero et al., 2002;  
133 Goudie & Middleton, 2006; Bullard et al., 2011; Querol et al., 2019). These basins encompass  
134 different sedimentary environments, many of which are potentially ~~efficient sources of~~ dust  
135 ~~emission hotspots~~, including unconsolidated aeolian deposits, endorheic depressions, and  
136 fluvial and alluvial dominated systems (Bullard et al., 2011). Consolidated or compacted fine  
137 sediments in the form of crusts and paved sediments, for instance on ephemeral lake beds, can  
138 also be important dust emitting surfaces when loose sand size sediments provided by adjacent  
139 sand dunes are available (Stout, 2003). These sand particles are efficiently mobilised by wind  
140 and ~~strike-blast~~ the consolidated surface breaking the sediment aggregates and releasing dust  
141 (Shao et al., 2011).

Con formato: Inglés (Estados Unidos)

Con formato: Fuente: Sin Cursiva

Con formato: Fuente: Sin Cursiva

Con formato: Fuente: Sin Cursiva

Con formato: Fuente: Sin Cursiva

Con formato: Inglés (Estados Unidos)

142 Models developed to simulate the atmospheric dust cycle and its impact on climate represent  
143 dust emission, transport, interactions with radiation and clouds, and removal by wet and dry  
144 deposition (Tegen and Fung, 1994; Ginoux et al., 2001; Zender et al., 2004; Perez et al., 2011,  
145 Klose et al., 2021). ~~Modelling efforts have mostly focused on the representation of dust sources~~  
146 ~~and emission (Kok et al., 2021) and~~ the characterization of dust sources ~~and hotspots~~ is one of  
147 the crucial aspects for representing dust mobilisation in models. ~~Traditionally~~Initially, models  
148 used ~~aridity-vegetation cover~~ as a criterion to identify potential dust sources (e.g. Tegen and  
149 Fung, 1994). Satellite retrievals subsequently showed that the most prolific sources occupy a  
150 smaller fraction of arid regions (Prospero et al., 2002; Ginoux et al., 2012). These so-called  
151 ~~hotspots or~~ “preferential sources” are found within enclosed basins, where easily eroded soil  
152 particles accumulate after fluvial erosion ~~and transport of~~ from the surrounding high-lands. The  
153 implementation of preferential source functions in global models based on topography (Ginoux  
154 et al., 2001), hydrology (Tegen et al. 2002; Zender et al. 2003), geomorphology (Bullard et al.,  
155 2011), or satellite proxies (Prospero et al., 2002; Ginoux et al., 2012), has significantly improved  
156 the skill of models by approximately locating large-scale natural sources ~~dust hotspots~~. However,  
157 models are not able yet to capture the small-scale spatial and temporal variability in emissions  
158 apparent from observations. ~~Some studies~~Models assume relatively homogeneous soil  
159 ~~properties everywhere due to the lack of data, - while- there can be an important~~significant  
160 ~~heterogeneity. Furthermore~~Some studies have provided small-scale understanding on the role  
161 of geomorphology and sedimentology upon dust emissions (Bullard et al., 2011; Baddock et al.,  
162 2016). For instance, Bullard et al. (2011) developed a conceptual model of how different  
163 geomorphologic surfaces affect the intensity and temporal variability in dust emissions.

164 While it is key to understand dust ~~source-hotspot~~ locations and emission intensity, climate  
165 impacts by dust also depend upon its mineralogy (Alshemmari et al., 2013). Dust is a mixture of  
166 different minerals including quartz, clay minerals (mica/illite, kaolinite, palygorskite,  
167 chlorite/clinochlore and smectite/montmorillonite), feldspars (albite/anorthite and orthoclase),  
168 carbonate minerals (mainly calcite and dolomite), salts (mainly halite and gypsum), Fe-oxides  
169 and hydroxides (mostly goethite and hematite) and other oxides or hydroxides of Ti, Mn and Al  
170 (Coudé-Gaussien et al., 1987; Schültz & Sebert, 1987; Molinaroli et al. 1993; Gomes, 1990; Sabre,  
171 1997; Caquineau, 1997; Avila et al., 1997; Caquineau et al, 1998; Claquin et al., 1999; Al-Ghadban  
172 et al., 1999; Cattle et al., 2002; Formenti et al., 2008; Nickovic et al., 2012; Alshemmari et al.,  
173 2013; Scheuven et al., 2013; Journet et al., 2014; Scanza et al., 2015; Subramaniam et al., 2015;  
174 Doronzo et al., 2016; Al-Dousari et al., 2018, 2019, 2020; Ito & Wagai, 2017; Querol et al., 2019).  
175 The relative abundances, size, shape, and mixing state of these minerals influence the effect of  
176 dust upon climate. For instance, the absorption of solar radiation by dust depends upon the iron  
177 oxide content (Tegen et al., 1997; Sokolik and Toon, 1999; Reynolds et al., 2014, Di Biagio et al.,  
178 2019), ice nucleation in mixed-phase clouds is highly sensitive to the amount of K-feldspar and  
179 quartz (Boose et al., 2016b; Harrison et al., 2019), and the bioavailability of iron in dust depends  
180 upon its iron mineralogy and speciation (Shi et al., 2012). ~~Recent studies have shown that cloud~~  
181 ~~pH is controlled in great part by calcite from dust (Grider et al., 2023). Furthermore, Ca is~~  
182 ~~controlling~~controls heterogeneous reactions of acids on the surface of dust, which ultimately  
183 ~~affect O3 production (Bauer et al., 2004; Paulot et al., 2016)~~. According to the geological,  
184 geomorphological and climate (weathering) patterns of the desert regions, the type, and  
185 proportions of minerals might greatly vary (Caquineau, 1997; Caquineau et al, 1998, Claquin et  
186 al., 1999; among others). For ~~example~~instance, Sahelian dust is composed mainly of quartz,

187 kaolinite and hematite, ~~the mineralogy~~ Middle Eastern dust is dominated by quartz and  
188 carbonates (Al-Dousari, 2018, 2019, 2020), ~~while and~~ in North-eastern China and the Sahara dust  
189 mica/illite, kaolinite, quartz and carbonates prevail (Shen et al., 2009; Claquin et al., 1999).

190 Despite the potential importance of dust mineralogical variations, climate models typically  
191 assume dust composition as globally uniform, which is partly due to ~~our~~ the limited knowledge  
192 of the composition of the parent sources at global scale. The few models that explicitly represent  
193 dust mineralogical composition (e.g., Scanza et al., 2015; Periwitz et al., 2015, Li et al., 2021;  
194 Gonçalves Ageitos et al., 2023) use global atlases of soil type and the relation of this variable to  
195 soil mineralogy. This relation is inferred using massive extrapolation from a limited amount of  
196 mineralogical analyses, particularly in dust ~~source regions~~ hotspots, ancillary information on soil  
197 texture and colour, and a number of additional assumptions (Claquin et al., 1999; Journet et al.,  
198 2014). ~~The mineralogical composition~~ Conventionally, the particle size of dust is ~~is~~  
199 characterized by measuring in two traditional ~~two particle grain~~ particle size ranges (Wentworth (1922)  
200 and Urquhart (1959)), i.e. clay (<2 µm) and silt (2-63 µm) linked to FAO (Food and Agricultural  
201 Organization of the United States) soil texture datasets based on measurements following wet  
202 sieving, a technique that disperses (breaks up) the mineral aggregates found in the undisturbed  
203 parent soil into smaller particles (Chatenet et al., 1996). Furthermore, the samples that underpin  
204 these atlases consider the first 10-15 cm of soil sediment, which is much deeper than the thin  
205 layer that is relevant to wind erosion and dust emission, and mineralogy is normally analysed  
206 after removing organic matter with hydrogen peroxide (H<sub>2</sub>O<sub>2</sub>), which can partially dissolve  
207 carbonate minerals.

208 The assumed relationship between mineralogy and soil type in these atlases neglects the role of  
209 geomorphology and sedimentology affecting the formation of different dust-emitting surface  
210 sediments, such as ~~dunes,~~ crusts, and paved sediments. ~~In this study,~~ we provide a  
211 comprehensive analysis of the variability in ~~grain size~~ particle size, mineralogical composition  
212 and Fe ~~mineralogy and speciation~~ mode of occurrence of sediments collected across the Lower  
213 Drâa Valley, an inland drainage basin and prolific dust-source located in the north-western  
214 border of the Saharan desert in southern Morocco (Figure 1). The data collection was ~~performed~~  
215 ~~carried out~~ during a ~~wind erosion and~~ dust field campaign in September 2019 in the context of  
216 the FRontiers in dust minerAlOGical coMposition and its Effects upoN climaTe (FRAGMENT)  
217 project. Based on the analysis of the results ~~we propose~~ a conceptual model ~~is proposed~~ that  
218 links formation processes of potential dust-emitting sediments to their ~~particle size~~ particle size  
219 distribution (PSD) and mineralogy across the basin.

220

## 221 2. Methodology

### 222 2.1 The FRAGMENT field campaign and the study area

223 The sediment samples analysed in this study were collected during a field campaign that took  
224 place in September 2019 in the Lower Drâa Valley, west of M'Hamid, between the Erg Chigaga  
225 and L'Bour (Figure 1a), a dry inland drainage basin where dust emission is frequent as evidenced  
226 by satellite data (Ginoux et al. 2012) (Figure 1b). The region lies where the Sahara Desert begins,  
227 to the south of the Atlas Mountain, near the Algerian border, in the Drâa River Basin. Preliminary  
228 results from the Earth Surface Mineral Dust Source Investigation, EMIT, (Green et al., 2020) show  
229 the presence of a complex regional mineralogy with fine-grained goethite, hematite (with

Con formato: Interlineado: Múltiple 1.15 lín.

230 substantial nano-sized hematite), gypsum sulphate salts in the lowlands (depressions) and  
231 Illite/muscovite, with local outcrops of carbonates in the study area (Figure 1c). The EMIT  
232 mineral maps show that the study area is representative of the larger area.

233 The campaign was conducted in the framework of the FRAGMENT project, in which distinct  
234 desert dust ~~source region~~ hotspot regions are being characterised to better understand the size-  
235 resolved dust emission and composition for different meteorological and soil conditions. The  
236 aim of FRAGMENT is to better understand dust emission, its mineralogical composition and the  
237 effects of dust upon climate, by combining field measurements, laboratory analyses, remote and  
238 in situ spectroscopy, theory and modelling. FRAGMENT field campaigns consist of intensive  
239 sediment sampling and meteorological and airborne dust measurements in one specific  
240 location, along with sediment sampling across the broader basin. The intensive meteorological  
241 and airborne dust measurements were performed in the dry lake L'Bour and are analysed in e.  
242 g., González-Florez et al., 2022; Panta et al., 2022; Yus et al., in prep. Here ~~the we~~ focus is on the  
243 sediment sampling across the basin.

244 The study area records very low annual precipitation (~~ranging from <50 to 800 mm~~ 80 mm) and  
245 extremely variable droughts interrupted by extreme floodings (Berger et al., 2021). The Drâa  
246 River was anthropogenically dried in this area mostly due to the construction of El Mansour  
247 Eddahbi dam in 1972 (near Ouarzazate). The Jbel Hassan Brahim range reaches the highest  
248 altitude in the area (840 m.a.s.l.), while the Drâa River is the lowest point (570 m.a.s.l.). The  
249 study region corresponds to a low relief alluvial system, unarmored and unincised according to  
250 Bullard et al. (2011). Rains are scarce, but sometimes they concentrate in the mountains (high-  
251 lands) and even more sporadically they can directly affect the area during convective storms,  
252 creating flash floods with a high sediment load canalised by torrents or wadis, such as wadi  
253 Latache (high-lands) (Figure 1a), which flood flat areas. In specific areas across the basin, highly  
254 sediment-loaded waters can be shortly ponded on the way to Drâa River in small depressions,  
255 such as dry Lake Iriki, Erg Smar or L'Bour (low-lands) (Figure 1a), among other areas, along the  
256 floodplain. Dunes are concentrated in small flat areas, near depressions, where, after wind  
257 erosion, sediment can be dragged and be entrapped by the very scarce and low vegetation.

## 258 2.2 Sediment sampling

259 The sampled sediments include paleo-sediments (hereafter named sediments), paved  
260 sediments, crusts, and dunes, according to the classification by Watt & Valentin (1992) and  
261 Valentin & Bresson (1992). Paved sediments result from cyclic drying and aeolian erosion of the  
262 surface of paleo-sediments and range from 0.5 to 2 cm of vertical depth. Crusts ranged from 0.1  
263 to 2 cm of vertical depth and ~~we differentiated~~ two types are differentiated: i) thin depositional  
264 crusts formed as result of the deposition of sediments from running water during floods, and ii)  
265 thicker sedimentation crusts resulting from the sedimentation and drying of highly sediment-  
266 loaded waters in ponded areas of different sizes. The difference between paved sediments and  
267 crusts is mostly the period of formation. The former dates from can date up to thousands of  
268 years ago, while the latter was formed recently. However, crust might have finer sediments  
269 because these are formed by ponding. Sediments are below the crusts (not exposed to the  
270 atmosphere) and dunes are aeolian deposits. ~~We used a~~ 50 cm<sup>2</sup> inox steel shovel was used to  
271 sample surfaces (first top cm), sediments (below surface, from 1 to 5 cm in the vertical depth)  
272 and dunes (from surface to 5 cm). ~~We registered c~~ Coordinates, type of sample, surroundings

Con formato: Párrafo de lista, Punto de tabulación: 0.5 cm, Izquierda

273 description, and ~~we also recorded~~ any other important information ~~were registered and made~~  
274 ~~concept drawings. We obtained~~ A total of 42 sediment samples ~~were obtained~~, including crusts  
275 (12), dunes (12), paved sediments (11) and sediments (7) (Figure 2) from different locations in  
276 the Drâa River Basin ~~(Figure S1). These were considered representative because the study~~  
277 ~~focuses on sediments (not deposited dust) and one basin.~~

### 278 2.3 Sample treatment

279 To analyse mineral-size fractionation (<10 and 10-63 µm), ~~we applied~~ a fully dispersed size  
280 fractionation using MilliQ-grade water and shaking the samples ~~was applied previous prior~~ to  
281 separation for 12-24 h. First, samples were subjected to 250, 63 and 10 µm sieves to obtain the  
282 <63 and <10 µm fractions. Due to availability, the smallest opening size of the sieve was 10 µm.  
283 Sonic sieving was applied for 60 s at maximum sustainable power for 3 min in every sieve. Finally,  
284 subsequent drying at 80 °C was applied to recover the solid fraction from the suspension.

### 285 2.4 Analysis

#### 286 2.4.1 ~~Particle size~~ Particle -size distribution and texture

287 The ~~particle size~~ particle -size analysis was carried out for fully (natural aggregates totally  
288 dispersed) and minimally (natural aggregates minimally dispersed) dispersed PSD to obtain the  
289 fully dispersed ~~particle size~~ particle -size distribution (FDPSD) and the minimally dispersed  
290 ~~particle size~~ particle -size distribution (MDPSD) to evaluate (i) how aggregates and particles occur  
291 in natural conditions (MDPSD) and (ii) the distribution of single particles that form the  
292 aggregates (FDPSD). The MDPSDs were obtained with laser diffraction using a Malvern  
293 Mastersizer 2000 Scirocco accessory (hereinafter, Scirocco) for minimally dispersed conditions.  
294 In this case, samples of 0.3-0.5 g of the fraction <2 mm were introduced into the Scirocco  
295 vibration plate with a 2 mm aperture and 5 s measuring time. FDPSDs were determined using  
296 the Malvern Mastersizer 2000 Hydro G accessory (hereinafter, Hydro) with a water suspension  
297 and ultrasound assistance for totally dispersed conditions. In that case, the samples were pre-  
298 treated following the method by Sperazza et al. (2004). The suspension was introduced into the  
299 Hydro's sample container, pumping at 1750 rpm and stirring at 500 rpm. Results were obtained  
300 in both cases using the Fraunhofer method (Etzler et al., 1997).

301 To investigate the possible occurrence of vertical segregation of the PSD (top layers are the ones  
302 that are emitting dust), 7 crust and 5 paved sediment samples were selected for vertically-  
303 resolved PSD analyses. To this end, 3 sub-samples were extracted from each sample (top,  
304 middle, and bottom sections) by scratching the surface with a cutter from top to bottom and  
305 were analysed separately. The thickness of these crusts varied between 4 to 8 mm.

306 The pipette method was also used to analyse the texture of a soil layer or boundary according  
307 to FAO-UNESCO (1990) of a total of six samples. This allows ~~us~~ to separate a suspension of the  
308 sample in MilliQ-grade water into different size fractions (>63, 2-63 and <2 µm), dry and analyse  
309 each size-fraction individually.

#### 310 2.4.2 Mineralogical composition

311 Quantitative mineralogical analyses of bulk sediment samples and segregated size fractions  
312 were carried out by means of powder X-Ray Diffraction (XRD), using a Bruker D8 A25 Advance,  
313 with Cu K<sub>α1</sub> radiation of 1.5405 Å wavelength, a Bragg Brentano geometry and a LynxEyeXE

314 detector. Analysis was performed at 40 mA and 40 kV with a range of angles from 4 to 60° and  
315 angle steps of 0.019° and 10 Hz for 1 h/sample. The mineral identification was made with the  
316 EVA software package by Bruker. For quantitative analyses ~~we used~~ the method of the internal  
317 reference material by Chung (1974) ~~was applied~~, with quartz as the internal reference. The ratios  
318 of intensities of the different minerals versus quartz were obtained by preparing and analysing  
319 binary mixtures of the specific minerals and quartz. The accuracy of the XRD quantitative  
320 approach was tested by analysing 16 mixtures of reference materials with known concentrations  
321 of minerals. Figure S24 summarises major results, which yield relative standard deviations  
322 versus the known contents of quartz (13 % of error), albite/anorthite (10 %), calcite (31 %),  
323 dolomite (14 %), mica/illite (29 %), kaolinite (11 %), gypsum (27 %), anhydrite (19 %), goethite  
324 (42 %), hematite (50 %).

325 For an in-depth evaluation of clay mineralogy, XRD analyses of oriented aggregates following  
326 the procedure by Thorez (1976) were carried out for the same six samples of the texture. ~~We~~  
327 ~~treat~~ ~~the~~ ~~samples~~ ~~were~~ ~~treated~~ for air drying (AO), glycolation (AG) and heating (AC).  
328 Mica/illite, chlorite/kaolinite, palygorskite and smectite were found in all the samples, as  
329 evidenced from the bulk XRD analysis. Calcite and dolomite were dissolved by acidifying soil  
330 suspension with a strong acid as HCl and the excess used to quantify stoichiometrically the  
331 content of carbonates using the method proposed by Horváth et al. (2005) also for the same six  
332 samples of the clay-oriented aggregates and texture.

333 To investigate the possible occurrence of mineralogical vertical segregation, the 7 crust and 5  
334 paved sediment unaltered samples used for ~~particle size~~ ~~particle~~ ~~-size~~ analysis (see section 2.4.1)  
335 were also used for vertically-resolved mineralogy analyses.

#### 336 2.4.3 Mode of occurrence of Fe

337 Fe is a key ingredient to climatic and biological processes affected by dust. For instance, the  
338 amount, mixing state and size of Fe-oxy/hydroxides determine the degree of absorption of solar  
339 radiation by dust (Engelbrecht et al., 2016) and the potential solubility of the dust deposited into  
340 the ocean (Shi et al., 2012). However, the XRD semiquantitative analysis for Fe-oxy/hydroxides  
341 are affected by large uncertainties due to the low concentrations (increasing relative errors) and  
342 is not sensitive to nano-Fe-oxides (Shi et al., 2012). ~~We complemented the~~ XRD analyses ~~were~~  
343 ~~complemented~~ by quantifying the levels and mode of occurrence of Fe in the bulk samples ~~using~~  
344 ~~the methodology~~ ~~as~~ described in Shi et al. (2009). ~~The method is based~~ ~~latter being based~~  
345 ~~through which based~~ on a sequential extraction ~~protocol to obtain the proportions of~~ ~~we~~  
346 ~~determine the amount of~~ readily exchangeable (adsorbed) Fe ions and ~~Fe in~~ nano-Fe-oxides  
347 (FeA) and the amount of ~~Fe in~~ crystalline Fe-oxides, mainly ~~from~~ hematite and goethite (FeD) in  
348 the samples, ~~were determined~~. ~~We used~~ 30 mg of Arizona Test Dust (ATD; ISO 12103-1, A1  
349 Ultrafine Test Dust; Powder Technology Inc.) ~~was~~ ~~ere~~ ~~used~~ to test the accuracy of the method  
350 and extractions were done with 15 ml of extractant solution. For total Fe content (FeT), ~~we used~~  
351 a two-step wet acid digestion method developed by Querol et al. (1993, 1997) and a coal fly ash  
352 (1633b) standard sample ~~was~~ ~~were~~ used to test accuracy. The 1633b gave 7.5 % with a standard  
353 deviation of 0.14 % for total Fe (reference content of 7.8 % of Fe), while ATD gave 0.076 % with  
354 a standard deviation of 0.002 % of FeA and 0.49 % with a standard deviation of 0.07 % for FeD +  
355 FeA (reference content of 0.067 % of FeA and 0.41 % of FeD). Furthermore, by subtraction, ~~we~~  
356 ~~obtained~~ the contents of structural Fe ( $FeS = FeT - (FeA + FeD)$ ) ~~were obtained~~, corresponding



357 to the Fe fraction as elemental Fe into the structure of minerals other than Fe-oxides, such as  
358 illite or other Fe-bearing minerals. Furthermore, the FeD contents were converted  
359 stoichiometrically to hematite ( $\text{Fe}_2\text{O}_3$ ) and goethite ( $\text{FeO}(\text{OH})$ ) by using the hematite/goethite  
360 proportions from XRD.

#### 361 2.4.5 Electron microscopy of crust and paved sediment sections

362 The PSD, mineralogy and morphology of crust and paved sediments can vary along the vertical  
363 profile, especially in crusts where progressive sedimentation and subsequent evaporation leads  
364 to inter-layering of sediments with different properties. For that purpose, crust and paved  
365 sediment sections were impregnated with epoxy resin, cut, and polished with diamond paste  
366 for microscopy analysis. The polished samples were coated with graphite before analysis with a  
367 JEOM JSM-7001F SEM-EDX Scanning Electron Microscope (SEM).

### 368 3. Results and discussion

#### 369 3.1 Regional variability

##### 370 3.1.1 Particle size distribution

371 ~~We analyse~~The PSDs of the samples collected across the basin ~~were analysed~~ to detect possible  
372 trends or size segregation patterns from high- to low-lands for the different types of sediment.  
373 The mean median diameter values of each group of sediments provided in this section represent  
374 the mean and standard deviation of the median diameters. Because the PSDs are generally bi-  
375 modal, other PSD metrics can be found in Table 1, including the maximum, minimum and mean  
376 of the median diameters for different types of sediments, location, PSD type (MDPSD and FDPS),  
377 and size fraction (full range,  $<63 \mu\text{m}$  and  $>63$  to  $< 2000 \mu\text{m}$ ).

378 MDPSDs, excluding dune samples, show a major mode centred around  $100 \mu\text{m}$  in diameter and  
379 a secondary one between 2 to  $20 \mu\text{m}$  (Figure 3a; Table 1). FDPSD's also show two modes at 5  
380 and  $100 \mu\text{m}$  (Figure 3b; Table 1). The MDPSDs and FDPSDs of dune samples are very similar with  
381 a main mode centred around  $150 \mu\text{m}$  and a secondary small one at  $5 \mu\text{m}$  (30 times lower) (Figure  
382 3c and d). Crust samples show the largest fine ( $0-5 \mu\text{m}$ ) fraction in MDPSD, followed by paved  
383 sediments and sediments (Figure 3e). FDPSDs show a similar trend but with a larger proportion  
384 of fine particles compared to MDPSD (Figure 3f).

385 The mean median diameter of the MDPSDs (Figure 4a), excluding dune samples, is  $88 \pm 63 \mu\text{m}$ ;  
386 and that of the FDPSDs, is  $27 \pm 51 \mu\text{m}$  (Figure 4a). Therefore, aggregates are about 3 times coarser  
387 than individual mineral particles. As expected, dunes were coarser than other types of  
388 sediments, with a mean median diameter of  $219 \pm 70 \mu\text{m}$  of the FDPSDs, which is very similar to  
389 that of the MDPSDs (Figure 4b). The mean median diameters of MDPSDs are  $70 \pm 48$ ,  $74 \pm 45$  and  
390  $113 \pm 79 \mu\text{m}$  for sediments, paved sediments and crusts, respectively (Figure 4c); whereas the  
391 mean diameters of FDPSDs are  $19 \pm 11$ ,  $21 \pm 26$  and  $37 \pm 77 \mu\text{m}$  for sediments, paved sediments  
392 and crusts respectively, about 3 to 4 times finer (Figure 4d).

393 The spatial variation of the mean diameter of the FDPSDs (Figure 5) shows coarser crusts ( $>40$   
394  $\mu\text{m}$ ) close to the high-land areas, and finer crusts ( $<40 \mu\text{m}$ ) near the Drâa River, likely due to  
395 flooding (causing transport and deposition of fine sediments, especially in the low-lands) caused  
396 during scarce and intensive rains. For paved sediments, sediments and dunes, spatial PSD trends

397 were not evident, with mean median diameters ranging from 10 to 120, 10 to 40 and 120 to 300  
398  $\mu\text{m}$ , respectively, randomly located across the basin (Table 1).

399 According to the size classification by Valentin & Bresson (1992) and using the FDPD data  
400 (Figure S32), dune samples can be classified as sand, loamy sand, and sandy loam; sediments as  
401 silt loam and loam; paved sediments as sandy loam, loam and silt loam; and crusts as sandy  
402 loam, loam, silty clay loam and silt loam. As shown in Figure S32 and due the higher transport  
403 potential of clays during rain episodes, and their accumulation during ponding, crusts tend to be  
404 further enriched in clay fractions, especially in low-lands, compared to paved sediments and  
405 sediment samples (see section 3.4).

### 406 3.1.2 Mineralogical composition

407 ~~We describe here~~ Here the mineralogy of samples collected across the basin ~~is described~~ to detect  
408 possible trends or mineral segregation patterns from high- to low-lands for the different types  
409 of sediment. The mineralogical composition (mass % composition of the bulk sample) of dunes,  
410 crusts, paved sediments and sediment samples is summarised in Table 2. Dunes show a  
411 homogeneous mineralogy across the study area, with mineral abundances of  $74\pm 9.7\%$  quartz,  
412  $5.8\pm 2.9\%$  calcite,  $6.7\pm 3.6\%$  microcline,  $6.9\pm 3.1\%$  albite/anorthite,  $4.1\pm 2.3\%$  clay minerals,  
413  $1.0\pm 1.4\%$  dolomite,  $0.38\pm 0.26\%$  goethite and  $0.12\pm 0.11\%$  hematite and trace amounts of halite  
414 and gypsum ( $<0.1\%$ ) (Figure 6). In comparison to dunes, crusts are depleted in quartz ( $48\pm 11\%$ )  
415 and feldspars ( $5.0\pm 2.1\%$  albite/anorthite and  $4.4\pm 3.1\%$  microcline), and enriched in clay  
416 minerals ( $17\pm 8.0\%$ ), calcite ( $19\pm 8.0\%$ ), dolomite ( $3.0\pm 1.3\%$ ) and Fe-oxides ( $0.24\pm 0.28\%$   
417 hematite and  $0.42\pm 0.56\%$  goethite) (Figure 6). The content of gypsum ( $0.23\pm 0.56\%$ ) and halite  
418 ( $2.9\pm 5.1\%$ ) is higher than in dune samples, but variability is large because it depends on the  
419 exact point of crust sampling. Paved sediments have a similar mineralogy than crusts, for quartz  
420 ( $51\pm 8.7\%$ ), calcite ( $17\pm 4.9\%$ ), clay minerals ( $16\pm 7.3\%$ ), albite/anorthite ( $6.3\pm 1.8\%$ ), microcline  
421 ( $4.5\pm 2.5\%$ ), dolomite ( $3.5\pm 0.79\%$ ), hematite ( $0.34\pm 0.25\%$ ), and goethite ( $0.38\pm 0.38\%$ ), but  
422 with lower content of gypsum ( $<0.1\%$ ) (Figure 6). Sediments are also similar to paved sediments  
423 and crusts with a mean quartz content ( $55\pm 11\%$ ), calcite ( $17\pm 4.6\%$ ), clay minerals ( $14\pm 6.8\%$ ),  
424 albite/anorthite ( $5.8\pm 1.5\%$ ), microcline ( $3.7\pm 1.6\%$ ), dolomite ( $3.4\pm 1.3\%$ ), hematite ( $0.28\pm 0.37\%$ )  
425 and goethite ( $0.37\pm 0.32\%$ ). Trace amounts of gypsum ( $<0.1\%$ ) and halite ( $0.32\pm 0.55\%$ ) were  
426 also found in sediments (Figure 6).

427 In comparison with the bulk sediment, the fully dispersed silt fraction ( $10\text{-}63\ \mu\text{m}$ ) shows a lower  
428 amount of quartz ( $35\pm 6.4\%$ ) and feldspars ( $7.4\pm 2.5\%$ ), a higher content of carbonates ( $25\pm 5.2\%$ )  
429 clays ( $22\pm 10\%$ ) and hematite ( $1.07\pm 0.38\%$ ) and a similar content of goethite ( $0.61\pm 0.32\%$ ).  
430 In the fully dispersed  $<10\ \mu\text{m}$  sieved fraction, the amount of quartz ( $23\pm 5.2\%$ ) and feldspars  
431 ( $4.7\pm 1.1\%$ ) is two times lower than in the bulk sediments. The fraction of carbonates remains  
432 similar ( $21\pm 9.0\%$ ) and the content of clays increases substantially ( $38\pm 9.8\%$ ) compared to the  
433 bulk and silt-size mineralogy. The Fe-oxide content increases by about a factor two for both  
434 hematite ( $2.2\pm 2.0\%$ ) and goethite ( $1.8\pm 1.2\%$ ). Table 3 compares ~~our the~~ mineralogical results  
435 in the clay and silt size ranges, both with the fully dispersed separation and the pipette methods,  
436 against the corresponding values provided by the available global mineralogical atlases of  
437 Claquin et al. (1999) and Journet et al. (2014), which assume ~~our the~~ sample locations to be  
438 either fluvisols or yermosols in terms of soil type. In the silt-size fraction, ~~we find~~ similar contents  
439 of quartz, total clay, mica/illite, chlorite+kaolinite, calcite and Fe-oxides, were found, but 3 times

440 less feldspars and 5 times more dolomite. Compared to the clay-size fraction in the atlases, ~~our~~  
441 ~~this study~~the <10 µm fraction ~~in this study~~, shows larger content of quartz and feldspars (by  
442 factor of 2 to 4), a 30 % lower total clay content and similar contents of calcite and Fe-oxides,  
443 which can only be partly explained by the difference in the size fraction considered (<10 µm vs  
444 <2 µm) as shown by the results obtained with the pipette method. Because kaolinite and chlorite  
445 have coincident spacing at 7 Å in the XRD spectra, in current atlases these minerals may be  
446 confounded, whereas in ~~our this study~~ ~~we quantified~~ chlorite was quantified separately by  
447 identifying other minor peaks in the spectra. This is relevant as both minerals are very different  
448 in terms of chemical composition. In ~~this our study~~, ~~we also detected~~ minor concentrations of  
449 dolomite and traces of smectite and palygorskite, were also detected. The large differences in  
450 the silt-size feldspar content may be largely due to the lack of data and coarse assumptions used  
451 in current atlases.

452 Table 4S1 in the supplemental material compares the silt+clay and sand proportions and the  
453 mineral contents of the crusts from this study in Morocco with those from deposited dust in  
454 different arid regions of the world. The FD-PSD data from this study evidences that 72% of the  
455 particles in the crusts fall in the clay+silt fraction (<63 µm), while 28% in the sand size-range.  
456 This is close to the average value (74 and 26%, respectively) calculated from the existing studies  
457 on deposited dust. Concerning the mineralogy, the crusts of this study are enriched in clays and  
458 depleted in carbonate minerals and feldspars compared with the average of the mineralogy of  
459 deposited dust shown in (Table 4S1).

460  
461 In ~~our this~~ analysis of trends in mineralogy from the high-lands to the low-lands, ~~we considered~~  
462 all sample types except dunes, were considered. The low-lands, such as L'Bour and Erg Smar,  
463 are enriched in clay minerals (17±9.6 and 14±3.4 %, respectively) compared to the high-lands  
464 (9.1±0.97 %) (Figure 6). Mica/illite is the most common clay mineral reaching mean contents of  
465 9.1±4.8, 8.1±2.0 in Erg Smar and L'Bour, respectively, and 5.0±0.70 % in the high-lands. Kaolinite  
466 reaches 7.2±5.4, 4.9±2.1 and 3.5±0.30 % and clinocllore 1.7±1.8, 1.3±0.67 and 0.49±0.38 %,  
467 respectively. Smectite and palygorskite were detected only in trace amounts (<0.1 %) in most  
468 samples, with only palygorskite at Erg Smar and high-lands reaching a mean content of  
469 0.34±0.58 and 0.15±0.06 %, respectively. The same trend is found for calcite (24±13, 16±3.1 and  
470 11±2.7 %, Erg Smar, L'Bour and high-lands), dolomite (5.0±5.1, 3.6±0.51 and 1.7±0.50 %, at Erg  
471 Smar, L'Bour and high-lands) and Fe-oxides (0.78±1.4, 0.37±0.43 and 0.08±0.04 % for hematite  
472 at Erg Smar, L'Bour and high-lands and 0.42±0.51, 0.39±0.35 and 0.32±0.21 % for goethite at Erg  
473 Smar, L'Bour and high-lands) being steeper for hematite than goethite (Figure 6). Quartz follows  
474 an opposite trend, increasing towards the high-lands (42±18, 53±5.0 and 61±5.4 %, at Erg Smar,  
475 L'Bour and high-lands, respectively) (Figure 6). Albite/anorthite and microcline do not show a  
476 clear trend, with 5.5±2.3, 5.9±1.8 and 5.4±1.2 % at Erg Smar, L'Bour and high-lands, and 3.4±2.4,  
477 5.0±3.4 and 4.6±1.7 %, respectively (Figure 6). Salt concentrations peak randomly and depend  
478 on very local scale conditions, being higher at concave areas where ponding is favoured (see  
479 section 3.4). The mean content of halite is 1.0±2.2, <0.1 and 4.0±7.7 % at Erg Smar, L'Bour and  
480 high-lands and that of gypsum is 0.18±0.35, <0.1 and 0.15±0.92 %, respectively (Figure 6).

481 A soft crust occurred on the surface of several dunes (Figure 2). The PSD and mineralogical  
482 analysis of the crust and the underlying sands did not reveal significant differences. Pye & Tsoar  
483 (2015) reported that surface hardening of dunes is due to the scavenging and deposition of clays

Con formato: Sin Resaltar

Con formato: Sin Resaltar

Con formato: Espacio Antes: 0 pto, Después: 6 pto

484 from suspended dust in light rains and by cementation of sand ~~grain~~particles (meniscus) by  
485 precipitation of carbonates and silica in the retained interstitial pore water. In both cases the  
486 potential variability caused by the slight increase of this clay and carbonate/silica cementation  
487 is obscured by variations in the bulk mineralogy.

### 488 3.2 Vertical segregation in crust and paved sediments

489 The examination of thin vertical cross-sections provides insight into how ~~particle size~~particle -  
490 size and mineral composition vary within the top few  $\mu\text{m}$  or mm of the surface. These differences  
491 are relevant to the mineralogy and PSD of newly emitted dust.

492 The MDPSDs of crust sections (top, middle and bottom) are very similar, with two modes of  
493 occurrence at 5-7 and 200  $\mu\text{m}$  (Figure S43a). Yet, while the FDPDSs show similar two modes at  
494 1-5 and 100  $\mu\text{m}$  for the top and middle sections and a second mode at 300  $\mu\text{m}$  for the bottom  
495 section (Figure S43b). The MDPSD mean median diameter of the 7 crust profiles reach  $25\pm 25$ ,  
496  $54\pm 80$  and  $25\pm 26$   $\mu\text{m}$  for the top, middle and bottom sections, respectively, while FDPDS means  
497 are  $9.4\pm 9.4$  and  $11\pm 9.5$   $\mu\text{m}$  in the top and middle sections and  $94\pm 145$   $\mu\text{m}$  in the bottom one  
498 (Figure S43c and d). Therefore, during the initial stages of ponding, coarser particles are  
499 deposited first while finer particles remain suspended (see section 3.4) in the later stages before  
500 evaporation of the water. Even some oxides, carbonates and salts may precipitate in the top  
501 layers of the crust as water evaporates and the ionic strength increases.

502 No vertical PSD segregation is observed in paved sediments, but some top sections analysed  
503 show enrichment in coarser fractions in FDPDS (the median diameter increases from bottom  
504 and middle sections ( $14\pm 6.8$  and  $12\pm 5.8$   $\mu\text{m}$ ) to the top section ( $23\pm 28$   $\mu\text{m}$ )), likely due to  
505 preferential erosion of finer fractions through sandblasting (see section 3.4).

506 The mean levels of quartz and feldspars are enriched in the bottom sections of the crusts ( $46\pm 17$   
507 and  $8.7\pm 4.6$  %, respectively) compared to the middle ( $38\pm 11$  and  $8.3\pm 2.5$  %) and top sections  
508 ( $41\pm 12$  and  $6.9\pm 2.2$  %) due to the higher quartz content of the coarse fraction that is deposited  
509 first (see section 3.4). The content of clay minerals, salts and Fe-oxides is similar in the top  
510 ( $20\pm 7.2$ ,  $<0.1$  and  $3.3\pm 1.9$  %, respectively), middle ( $21\pm 5.0$ ,  $<0.1$  and  $2.8\pm 1.6$  %), and bottom  
511 sections ( $19\pm 9.1$ ,  $<0.1$  and  $1.9\pm 1.0$  %). Carbonate minerals are relatively homogeneous, but  
512 slightly enriched in the middle and top sections ( $29\pm 9.7$  and  $28\pm 7.9$  %, respectively) compared  
513 to the bottom section ( $24\pm 8.4$  %). This can arise from both detrital carbonate particles and  
514 precipitation from high ionic strength waters that are ponded and dried in the low-lands.

515 The mineral composition of the paved sediment profiles differs slightly from that of crust  
516 profiles. This is because the latter are affected by particle segregation during transport and  
517 subsequent sedimentation. The top section of the paved sediment profiles has more quartz than  
518 in the middle and bottom sections ( $44\pm 8.1$ ,  $38\pm 5.7$  and  $40\pm 9.8$  %, respectively), whereas  
519 feldspars decrease from the bottom and middle to the top sections ( $9.1\pm 4.2$ ,  $9.3\pm 2.2$  and  $6.9\pm 2.7$   
520 %). Carbonates and clay are relatively homogeneous ( $26\pm 4.9$ ,  $26\pm 2.0$  and  $25\pm 4.2$  % for  
521 carbonates, and  $22\pm 8.4$ ,  $23\pm 9.2$  and  $25\pm 4.9$  % for clays, respectively). The slight depletion of  
522 minerals in the top section may be due to sandblasting, which tends to erode the fine fraction  
523 of the surface over time (see section 3.4). Fe-oxides are more present in the top section than in  
524 the middle and bottom sections ( $2.1\pm 0.47$ ,  $2.0\pm 0.38$  and  $1.7\pm 0.27$  %, respectively) and the  
525 presence of salts is very low ( $<0.1$  % for all sections).

### 526 3.3 Mode of occurrence of Fe

527 ~~We implemented a~~ sequential Fe extraction procedure ~~was implemented~~ to evaluate the levels  
528 and mode of occurrence of Fe in dust samples from the basin. Due to limitations of XRD analysis  
529 for low Fe-oxide contents, this procedure provided a much more precise quantitative evaluation.

530 The mean FeT content of bulk crusts, paved sediments and sediments was found to be  $3.6\pm 0.71$ ,  
531  $3.4\pm 0.47$ , and  $3.2\pm 0.44$  %, respectively, while bulk dunes had a much lower FeT content  
532 ( $2.0\pm 0.33$  %). Fe-speciation studies reveal that FeS percentage from FeT (FeS/FeT) is the  
533 prevailing Fe mode of occurrence ( $67\pm 2.4$ ,  $69\pm 3.0$ ,  $68\pm 2.7$  and  $73\pm 5.9$  % in crusts, paved  
534 sediments, sediments and dunes, respectively), followed by FeD percentage from FeT (FeD/FeT)  
535 ( $31\pm 2.3$ ,  $29\pm 3.0$ ,  $30\pm 3.0$ ,  $26\pm 5.8$  %), and FeA percentage from FeT (FeA/FeT) ( $1.9\pm 0.55$ ,  $1.7\pm 0.56$ ,  
536  $1.4\pm 0.55$  and  $1.0\pm 0.54$  %). These results show that FeT is very similar between crusts, paved  
537 sediments and sediments while FeT in dunes is depleted by almost 50 %. Compared to Shi et al.  
538 (2011) samples from northwestern Africa, ~~our the samples of this study are~~ depleted in total  
539 iron ( $4.7$  % FeT from Shi et al. (2011)), quite similar in FeS ( $67$  % from Shi et al. (2011)), similar in  
540 FeD ( $33$  % from Shi et al. (2011)) and much higher in FeA ( $0.43$  % from Shi et al. (2011)).

541 The mean FeT content in the basin is similar in Erg Smar ( $3.6\pm 0.27$  %) and L'Bour ( $3.2\pm 0.66$  %)  
542 compared to high-lands ( $3.0\pm 0.24$  %). The ratio FeA/FeT was slightly higher at Erg Smar ( $1.9\pm 0.53$   
543 %) but similar at L'Bour and high-lands ( $1.3\pm 0.44$  and  $1.5\pm 0.47$  %, respectively). This is probably  
544 due to the preferential accumulation of exchangeable and nano-Fe-Oxides (FeA) in the low-  
545 lands, where flooding results in red-water ponds and red surfaces after drying. Subsequently,  
546 highly concentrated ionic Fe is trapped in the last stages of ponding, and nano-Fe-oxides may  
547 precipitate during drying. Once the ponded is dried, the crusts of the low-lands tend to have a  
548 reddish patina (see section 3.4). However, a slightly higher mean FeD/FeT of  $33\pm 2.4$  % is  
549 obtained in the high-lands compared to  $31\pm 2.7$  and  $29\pm 2.4$  % at L'Bour and Erg Smar,  
550 respectively. The FeS/FeT mean content is slightly lower at the high-lands ( $65\pm 2.5$  %) compared  
551 to Erg Smar and L'Bour ( $69\pm 2.6$  and  $68\pm 2.6$  %, respectively).

552 FeD levels were apportioned between hematite and goethite using XRD proportions. These  
553 results show that in crusts,  $0.79\pm 0.66$  % of hematite and  $0.55\pm 0.67$  % of goethite are present, in  
554 paved sediments  $0.83\pm 0.51$  and  $0.64\pm 0.54$  %, in sediments  $0.73\pm 0.58$  and  $0.69\pm 0.59$  %, and in  
555 dunes  $0.20\pm 0.17$  % and  $0.68\pm 0.24$  %.

556 The proportions of FeD + FeA are higher in crusts, probably due to preferential transport of non-  
557 FeS to the low-lands and the trapping of Fe ions (FeA) by clay adsorption during ponding, and  
558 the formation of nanosized Ferrihydrite ( $\text{Fe}_{4-5}(\text{OH},\text{O})_{12}$ ). This readily exchangeable Fe has very low  
559 impact on radiative forcing but a high impact in Fe fertilisation of oceans during dust events  
560 (Gobler et al., 2001), as ionic Fe adsorbed by clays and nano-Fe-oxides are easily released in  
561 water solutions. The correlation of FeS, FeD and FeA with FeT is linear, with coefficients of  
562 determination ( $R^2$ ) reaching 0.96, 0.89 and 0.67 for FeS, FeD and FeA respectively (Figure S54).  
563 Thus, when increasing total Fe content all modes of occurrence of Fe increase, but the increase  
564 is preferentially driven by FeS, while it seems that the basin FeA segregation causes a lower  
565 correlation with FeT.

566 **3.4 Conceptual model for grain sizeparticle -size and mineralogy fractionation in crusts and**  
567 **paved sediments**

568 According to Bullard et al. (2011) and as previously discussed in this study, heavy rainfall results  
569 in the selective deposition of coarser particles from runoff and floodwaters in higher elevations.  
570 Conversely, smaller particles enriched in clays, colloidal Fe-oxides (which give the water a  
571 reddish hue), and dissolved salts tend to be transported to lower elevations. Figure 7  
572 summarises a conceptual model that outlines the formation of crusts and paved sediment in the  
573 study area, with a focus on particle sizeparticle -size and mineralogical fractionation.

574 In the low-lands, floodwaters carrying fine sediments flood extensive flat areas, such as Erg Smar  
575 or Iriki lake. Prospero et al. (2002), Bullard et al (2011) and Ginoux et al (2012), among others,  
576 have shown that dust emissions originate from relatively small and localised areas where  
577 sediments are supplied by floodwaters, and that the occurrence of dust emissions from these  
578 areas may be partly due to the occurrence or absence of floodings. During ponding in low-lands,  
579 coarser particles deposit first and form a high sand-rich bottom layer of the crust (as described  
580 in section 3.2) (Figure 7a & 8a). Subsequently, the clay fraction deposits on top of the bottom  
581 layer until total dryness (Figure 7a & 8a) forming a second clay-rich fraction layer in the crust.  
582 However, the particle sizeparticle -size in crust surfaces is heterogeneous (Figure S65 & S76),  
583 which can result in erodible dust-emitting sediment (heterogeneity enhances sandblasting). The  
584 finer and more easily exchangeable FeA fraction remains in suspension until the last drying  
585 stages on the most superficial layer of the crust, during drying out of the remaining ponds (as  
586 described in section 3.3) (Figure 7a & 8a). During this ponding, dissolved Fe ions interact with  
587 clays in such a way that they can be adsorbed on clay surfaces according to the ionic composition  
588 of the waters (as described in section 3.3) (Echeverría et al., 1998). This typical ion adsorption  
589 by clays is higher for montmorillonite than for other clays but the content of montmorillonite is  
590 low compared to illite. In this study a high correlation is obtained for FeA and illite contents  
591 (Figure S87). Furthermore, crusts contain a higher proportion of  
592 hematite(oxide)/goethite(hydroxide) in the FeD, due to the weathering with water during  
593 transport and ponding and precipitation of nano-Fe-oxides during drying.

594 After the pond drying, the continuous heating of the clay rich surface layer causes the hardening  
595 of the crust and mud-cracking, giving a 'ceramic-like' compactness to the thick crusts in the low-  
596 lands, usually with a reddish colour induced by the Fe-oxides (Figure S65a). Complete drying  
597 causes mud cracks due to loss of volume, breaking the crust into polygonal pieces, whose  
598 thickness and area depend on the amount of clay deposited. Furthermore, these concave mud-  
599 crust pieces resulting from the cracking usually have a grey-colour patch in the middle due to  
600 the superficial precipitation of salts, which together with carbonates accumulate by capillarity  
601 (see section 3.1.2) (Figure S65b). This capillary ascension and precipitation of salts (the latter  
602 being an expansive process) causes sponging and breaking of the surface layers. Thus, a third  
603 (top) layer is formed in the crusts of the low-lands, which is very easily eroded by wind because  
604 of the spongy structure and enriched in clay and readily exchangeable Fe. In some cases, in Erg  
605 Smar, ~~we observed~~ an additional breaking and sponging of the third (upper layer) due to  
606 expansive clays, was observed. Both the ceramic-like compactness and the cementing of salts  
607 give the fine-clay rich crusts in the low-lands a compact pattern with coarser MDPSD compared  
608 with the high-lands where ponding is limited and very thin crusts occur. This could explain why

609 the crusts from the low-lands have finer FDPDs and coarser MDPSDs compared to the high-  
610 lands (see section 3.1.1). Also, wind erosion of the few top millimetres of these crusts may result  
611 in dust with higher contents of clay, Fe-oxide and salts compared to a 15 cm sediment profile.

612 In the high-lands, washout erosion occurs during rainfall, leading to the formation very thin  
613 crusts in reduced areas. This results in sources of dust made of very thin crusts and fields of  
614 stony surfaces with lower emission rates compared to the low-lands (Bullard et al., 2011). As  
615 illustrated in Figure S76 the surfaces of paved sediments and their thin crusts might resemble  
616 crusts profiles, but with the top section depleted on clay minerals due to preferential erosion  
617 over time, and with a very thin layer (a few micrometres) of clay minerals from the previous  
618 intact formed crust after flooding or running water. The top paved sediments are more compact,  
619 finer and have homogeneous distribution of the particle than crusts, which makes them less  
620 erodible and less likely to emit dust compared to crusts (which have heterogeneous ~~particle~~  
621 ~~size~~particle-size, see section 3.2).

#### 622 4. Conclusions

623 This study analysed the ~~particle-size~~particle -size and mineralogy of dust-emitting sediments in  
624 the region of Drâa basin in Northern Africa, at the ~~northwestern~~north-western fringe of the  
625 Sahara. The study aimed to compare these patterns for different types of dust-emitting  
626 sediments and their variations across the basin. The results are consistent with the conceptual  
627 models of dust emission sources in desert areas of Prospero et al. (2002) and Bullard et al.  
628 (2011), which predict higher dust emissions in the low-lands than in the high-lands. The study  
629 shows a clear size and mineralogical fractionation between paleo-sediments and low-land dust-  
630 emitting sediments, indicating that collecting samples of parent paleo-sediments for ~~particle~~  
631 ~~size~~particle -size and mineralogy may not fully represent the ~~highly-emitting-dust~~ emission  
632 ~~sources~~hotspots.

633 Both PSDs and mineralogy are segregated by transport and deposition of sediments during  
634 runoff of water across the basin, and by the precipitation of salts, which causes a sedimentary  
635 fractionation. Coarser particles such as quartz, feldspars, and carbonates (detrital) deposit first  
636 due to friction and gravity and are enriched in high-lands. In contrast, waters reaching the low-  
637 lands are enriched in fine particles (clays), carbonate, salt and Fe ions from partial dissolution of  
638 minerals of the source lands. When these waters are ponded in low-lands, coarser minerals  
639 deposit first, followed by a second layer enriched in clays minerals. Evaporation of the last  
640 ponded water layer causes the deposition of the finest particles and clays enriched in readily  
641 exchangeable ions of Fe. Once dried, the heating of the surfaces by insolation causes  
642 evaporation of interstitial solutions moving towards the surface by capillarity, leading to the  
643 precipitation of salts and secondary carbonates in the upper layer. This expansive process  
644 sponges the surface of the crust, in some cases accelerated by the occurrence of expansive clays,  
645 which might favour dust emission from a top clay-Fe-salts rich micro-layer. Therefore, dust  
646 emission is not only higher but also has a different mineral composition in the low-lands than in  
647 high-lands that is also controlled by the type of sediment.

648 ~~Our~~ The results of this study~~results~~ show that modeling mineral-speciated dust emission  
649 requires understanding of ~~the~~ the mineralogical and particle -size fractionation of accumulated



650 sediments across inland enclosed basins. Large areas may act as sediment suppliers, while  
651 reduced areas may act as dust emitters with differences in sediment composition. Models that  
652 represent mineral-speciated dust emission and transport should be developed to properly  
653 account for these factors.

654 ~~Our~~The results have also shown that global atlases ~~fail to describe the clay size fraction of dust-~~  
655 ~~emitting sediments in the region,~~ overestimate~~ing~~ the clay mineral content and  
656 ~~underestimating~~ underestimate that of quartz, feldspars, and Fe-oxides. Quartz and feldspars  
657 are overestimated and clay minerals underestimated in the silt-size fractions. Kaolinite-chlorite  
658 are not differentiated, while ~~our~~this study ~~observes~~ finds major differences. The classical  
659 procedure loses salts during fractionation, and Fe-oxides are detected mainly by colour without  
660 precision. ~~Our~~This study detects dolomite, palygorskite, and smectite, and provides more  
661 precision for Fe-oxides, with the mode of occurrence of Fe in different types of samples and  
662 locations. However, the study was unable to obtain a sample below 10 µm without losing salts  
663 in the process.

664 Dust models need global observationally constrained high-resolution mineral maps, which will  
665 soon become available based on high-quality spaceborne spectroscopy measurements  
666 performed from the International Space Station (Figure 1c, Green et al., 2020). A key challenge  
667 of mineral mapping based on spectroscopy for dust emission modeling is to constrain not only  
668 the presence (Figure 1c) but also the abundance of the different surface minerals. The data  
669 gathered and ~~analysed~~ analyzed in this study will be used to evaluate these spaceborne  
670 retrievals in forthcoming studies.

671 The large dam built in the Drâa River has caused the drying of this part of the basin, a reduction  
672 of vegetation and probably increased dust emissions. The region exemplifies how anthropogenic  
673 activities can promote wind erosion and represents a unique location for research on the topic.  
674 Future studies may indeed explore many other aspects related to sedimentology, mineralogy,  
675 wind erosion, dust emission and anthropogenic impacts, including the study of the introduction  
676 of native plants and green belts to reduce wind erosion as has already been done in other  
677 regions (Al-Dousari et al. 2020).

678  
679  
680  
681  
682  
683  
684  
685  
686  
687  
688

**Con formato:** Fuente: Sin Negrita, Inglés (Estados Unidos)

**Con formato:** Fuente: Sin Negrita, Inglés (Estados Unidos)

**Con formato:** Fuente: Sin Negrita, Inglés (Estados Unidos)

**Con formato:** Fuente: Sin Negrita, Inglés (Estados Unidos)

**Con formato:** Fuente: Sin Negrita, Inglés (Estados Unidos)

**Con formato:** Fuente: Sin Negrita, Inglés (Estados Unidos)



689  
690  
691  
692  
693  
694  
695

696 **Acknowledgments**

697 The field campaign and its associated research, including this work, was primarily funded by the  
698 European Research Council under the Horizon 2020 research and innovation programme  
699 through the ERC Consolidator Grant FRAGMENT (grant agreement No. 773051) and the AXA  
700 Research Fund through the AXA Chair on Sand and Dust Storms at BSC. **CGF** was supported by a  
701 PhD fellowship from the Agència de Gestió d'Ajuts Universitaris i de Recerca (AGAUR) grant  
702 2020\_FI B 00678. **KK** was funded by the Deutsche Forschungsgemeinschaft (DFG, German  
703 Research Foundation) – 264907654; 416816480. **MK** has received funding through the  
704 Helmholtz Association's Initiative and Networking Fund (grant agreement no. VH-NG-1533).

705 ~~We~~The authors acknowledge the EMIT project, which is supported by the NASA Earth Venture  
706 Instrument program, under the Earth Science Division of the Science Mission Directorate. ~~We~~  
707 The authors thank Dr. Santiago Beguería from the National Scientific Council of Spain for  
708 facilitating a field site in Zaragoza, Spain, to test ~~our~~the field instrumentation and ~~field~~  
709 ~~procedures~~prior to our ~~the campaign in Morocco~~campaign in Morocco. ~~We~~The authors thank  
710 Paul Ginoux for providing high-resolution global dust source maps, which were very helpful for  
711 the identification of the FRAGMENT experimental sites. ~~We~~The authors thank Prof. Kamal Taj  
712 Eddine from Cady Ayyad University, Marrakesh, Morocco for his invaluable support and  
713 suggestions for the preparation of the field campaign. ~~We~~The authors thank Prof. Bethany L.  
714 Ehlmann and Dr. Rebecca Greenberger for the help collecting samples, doing infrared in situ  
715 spectroscopy and discussion analysis and to PhD. Abigail M. Keebler for discussion analysis. ~~We~~  
716 The authors thank Houssine Dakhamat and the crew of Hotel Chez le Pacha in M'hamid El  
717 Ghizlane for their support during the campaign.

718 **Credit authorship contribution statement**

719 **CPG-P** proposed and designed the field campaign with contributions of **AA, KK, MK and XQ**. The  
720 Campaign was implemented by **CPG-P, AA, CGF, AGR, KK, MK, AP, XQ, CR** and **JYD**. The samples  
721 were collected by **CPG-P, AA, AGR, MK and XQ** and analysed by **CB, PC, AGR, CR** and **ZS**.  
722 Spectroscopy was analysed by **RNC**. **AGR** performed the visualization and writing of the original  
723 draft manuscript and **CPG-P** and **XQ** supervised the work. **CPG-P** and **XQ** re-edited the  
724 manuscript and all authors contributed in data discussion, reviewing and manuscript finalization.

725

726 **Declaration of competing interest**

Con formato: Interlineado: Múltiple 1.15 lín.

727 Some authors are members of the editorial board of journal ACP. The peer-review process was  
728 guided by an independent editor, and the authors have also no other competing interests to  
729 declare.

730

## 731 5. References

732 [Al-Dousari A., Ibrahim M.I., Al-Dousari N., Ahmed M., Al-Awadhi S.: Pollen in aeolian dust with  
733 relation to allergy and asthma in Kuwait. \*Aerobiologia\*, 34, 325-336, 2018.](#)

734 [Al-Dousari A., Alsaleh A., Ahmed M., Misak R., Al-Dousari N., Al-Shattji F., Elrawi M., William T.:  
735 Off-road vehicle tracks and grazing points in relation to soil compaction and land  
736 degradation. \*Earth Syst. Environ.\*, 3, 471-482, 2019.](#)

737 [Al-Dousari A., Ramadan A., Al-Qattan A., Al-Ateeqi S., Dashti H., Ahmed M., Al-Dousari N., Al-  
738 Hashash N., Othman A.: Cost and effect of native vegetation change on aeolian sand, dust,  
739 microclimate and sustainable energy in Kuwait. \*J. of Taibah Univ. for Sci.\*, 14, 628-639, 2020.](#)

740 [Al-Ghadban A.N., Saeed T., Al-Dousari A., Al-Shemmari H., Al-Mutairi M.: Preliminary assesment  
741 of the impact of draining of iraqi marshes on kuwait's northern marine environment. parti.  
742 Physical manipulation. \*Water Science and Technology\*, 40, 7, 75-87, 1999.](#)

743 [Alshemmari H., Al-Dousari A., Talebi L., Al-Ghadban A.N.: Mineralogical characteristics of surface  
744 sediment in Sulaibikhat Bay, Kuwait. \*Kuwait J. of Science\*, 40, 2, 2013.](#)

745 [Avila A., Queralt I., Alarcón M.: Mineralogical composition of African dust delivered by red rains  
746 over northeastern Spain. \*Journal of Geophysical Research\* 102, D18, 21977-21996, 1997.](#)

747 Baddock M.C., Ginoux P., Bullard J.E., Gill T.E.: Do MODIS-defined dust sources have a  
748 geomorphological signature?. *Geophys. Res. Lett.*, 43, 2606-2613, 2016.  
749 doi:10.1002/2015GL067327

750 [Bauer, S.E., Balkanski, Y., Schulz, M., Hauglustaine, D.A. Dentener, F., 2004. Global modeling of  
751 heterogeneous chemistry on mineral aerosol surfaces: Influence on tropospheric ozone  
752 chemistry and comparison to observations. \*Journal of Geophysical Research: Atmospheres\*,  
753 109 D2, <https://doi.org/10.1029/2003JD003868>](#)

754 Berger E., Bossenbroek L., Beermann A.J., Schäfer R.B., Znari M., Riethmüller S., Sidhu N.,  
755 Kaczmarek N., Benaissa H., Ghamizi M., Plicht S., Salem S.B., El Qorchi F., Naimi M., Leese  
756 F., Frör O.: Social-ecological interactions in the Draa River Basin, southern Morocco:  
757 Towards nature conservation and human well-being using the IPBES framework. *Science of  
758 The Total Environment*, 769, 144492, ISSN 0048-9697,  
759 <https://doi.org/10.1016/j.scitotenv.2020.144492>, 2021.

760 Boose Y., Sierau B., García M.I., Rodríguez S., Alastuey A., Linke C., Schnaiter M., Kupiszewski P.,  
761 Kanji Z.A., Lohmann U.: Ice nucleating particles in the Saharan Air Layer. *Atmospheric  
762 Chemistry and Physics*, 16, 14, 9067-9087, 2016.

763 Boyd P.W., Jickells T., Law C.S., Blain S., Boyle E.A., Buesseler K.O., Coale K.H., Cullen J.J., De Baar  
764 H.J.W., Follows M., Harvey M., Lancelot C., Levasseur M., Owens N.P.J., Pollard R., Rivkin  
765 R.B., Sarmiento J., Schoemann V., Smetacek V., Takeda S., Tsuda A., Turner S., Watson A.J.:  
766 Mesoscale Iron Enrichment Experiments 1993-2005: Synthesis and Future Directions.  
767 *Science*, 315, 612-617, 2007.

768 Bullard J.E., Harrison S.P., Baddock M.C., Drake N., Gill T.E., McTainsh G., Sun Y.: Preferential  
769 dust source: A geomorphological classification designed for use in global dust-cycle models.  
770 *J. of Geoph. Res.*, vol. 116, F04034. doi: 10.1029/2011JF002061, 2011.

771 [Caquineau S.: Les sources des aérosols sahariens transportés au-dessus de l'Atlantique tropical  
772 nord: Localisation et caractéristiques minéralogiques. Ph.D. thesis, Univ. Paris 12, 1997.](#)

773 Caquineau S., Gaudichet A., Gomes L., Magonthier M.C., Chatenet B.: Saharan dust: Clay ratio as  
774 a relevant tracer to assess the origin of soil derived aerosols. *Geophysical Research Letters*,  
775 25, 7, 983-986., 1998.

776 [Cattle S.R., McTainsh G.H., Wagner S.: Aeolian dust contributions to soil of the Namoi Valley,  
777 northern NSW, Australia. \*Catena\*, 47, 3, 245-264, 2002.](#)

Con formato: Inglés (Reino Unido)

Con formato: Inglés (Reino Unido)

Con formato: Inglés (Reino Unido)

Con formato: Inglés (Reino Unido)

Con formato: Inglés (Reino Unido)

Con formato: Subrayado

Con formato: Inglés (Reino Unido)

Con formato: Inglés (Reino Unido)

778 Chung F.H.: Quantitative Interpretation of X-Ray Diffraction Patterns of Mixtures. I. Matrix-  
779 Flushing Method for Quantitative Multicomponent Analysis. Journal of Applied  
780 Crystallography, Vol. 7, 519-525, 1974.

781 Claquin T., Schulz M., Balkanski Y.J.: Modeling the mineralogy of atmospheric dust sources.  
782 Journal Geophysical Research. 104, D18, 22243-22256, 1999.

783 Clark R.N., Swayze G.A., Livo K.E., Kokaly R.F., Sutley S.J., Dalton J.B., McDougal R.R., and Gent  
784 C.A.: Imaging spectroscopy: Earth and planetary remote sensing with the USGS Tetracorder  
785 and expert systems. Journal of Geophysical Research, Vol. 108(E12), 5131,  
786 doi:10.1029/2002JE001847, p. 5-1 to 5-44, 2003.

787 Clark R.N.: Tetracorder source code on github. [https://github.com/PSI-edu/spectroscopy-](https://github.com/PSI-edu/spectroscopy-tetracorder)  
788 [tetracorder](https://github.com/PSI-edu/spectroscopy-tetracorder). 2023.

789 Chatenet B., Marticorena B., Gomes L., Bergametti G.: Assessing the microped size distributions  
790 of desert soils erodible by wind. Sedimentology, 43, 5, 901-911, 1996.

791 ~~Coudé-Gaussen G., Rognon P., Bergametti G., Gomes L., Strauss B., Gros J. M., Le Coustumer~~  
792 ~~M.N.: Saharan dust over Fuerteventura Island (Canaries), Chemical and mineralogical~~  
793 ~~characteristics, air mass trajectories and probable sources. Geophys. Res. 92, 9753-9771,~~  
794 ~~1987.~~

795 De Longueville F., Hountondji Y. C., Henry S., Ozer P.: What do we know about effects of desert  
796 dust on air quality and human health in West Africa compared to other regions?. Sci. Total  
797 Environ., 409, 1-8, 2010.

798 Di Biagio C., Formenti P., Balkanski Y., Caponi L., Cazaunau M., Pangui E., Journet E., Nowak S.,  
799 Andreae M.O., Kandler K., Saeed T., Piketh S., Seibert D., Williams E., Doussin J.-F.: Complex  
800 refractive indices and single-scattering albedo of global dust aerosols in the shortwave  
801 spectrum and relationship to size and iron content. Atmos. Chem. Phys., 19, 15503-15531,  
802 <https://doi.org/10.5194/acp-19-15503-2019>, 2019.

803 [Doronzo D.M., Al-Dousari A., Folch A., Dagsson-Waldhauserova: Preface to the Dust Topical](https://doi.org/10.1007/s12517-016-2504-9)  
804 [Collection. Arab. J. Geosci., 9, 468, 2016. https://doi.org/10.1007/s12517-016-2504-9](https://doi.org/10.1007/s12517-016-2504-9)

805 ~~Dubief J.: Review of the North African climate with particular emphasis on the production of~~  
806 ~~aeolian dust in the Sahel zone and in the Sahara, in Saharan Dust: Mobilization, Transport,~~  
807 ~~Deposition, edited by C. Morales, 27-48, Wiley, New York, 1977.~~

808 Echeverría J.C., Morera M.T., Mazkiarán C., Garrido J.J.: Competitive sorption of heavy metal by  
809 soils. Isotherms and fractional factorial experiments. Environmental Pollution, 101, 2, 275-  
810 284, ISSN 0269-7491, [https://doi.org/10.1016/S0269-7491\(98\)00038-4](https://doi.org/10.1016/S0269-7491(98)00038-4), 1998.

811 Engelbrecht J.P., Moosmüller H., Pincock S., Jayanty R.K.M., Lersch T., Casuccio G., Technical  
812 note: Mineralogical, chemical, morphological, and optical interrelationships of mineral dust  
813 re-suspensions. Atmos. Chem. Phys., 16, 10809-10830, doi:10.5194/acp-16-10809-2016,  
814 2016.

815 Etzler F.M. and Deanne R.: Particle Size Analysis: A comparison of Various Methods II. Part. Part.  
816 Cyst. Charact., 14, 278-282, 1997.

817 FAO-UNESCO: Food & Agriculture Organization-United Nations Educational Scientific, and  
818 Cultural Organization: Guidelines for soil description, 3<sup>rd</sup> edition, Journal FAO & ISRIC,  
819 Rome, 1990.

820 Formenti P., Rajot L., Desboeufs K., Caquineau S., Chevaillier S., Nava S., Gaudichet A., Journet  
821 E., Triquet S., Alfaro S., Chiari M., Haywood J., Coe H., Highwood E.: Regional variability of  
822 the composition of mineral dust from western Africa: Results from the AMMA SOPO/DABEX  
823 and DODO field campaigns. J. Geophys. Res. 113, D00C13, doi:10.1029/2008JD009903,  
824 2008.

825 [Gillette, D. A. \(1999\), A qualitative geophysical explanation for hot spot dust emitting source](#)  
826 [regions, Contrib. Atmos. Phys., 72, 67-77.](#)

827 Ginoux P., Chin M., Tegen I., Prospero J.M., Holben B., Dubovik O., Lin S.-J.: Sources and  
828 distributions of dust aerosols simulated with the GOCART model. Journal of Geophysical  
829 Research: Atmospheres, 106, D17, 20255.20273, 2001.

Con formato: Inglés (Reino Unido)

Con formato: Fuente: Sin Cursiva

830 Ginoux, P., Prospero J.M., Gill T.E., Hsu N.C., Zhao M.: Global-scale attribution of anthropogenic  
831 and natural dust sources and their emission rates based on MODIS Deep Blue aerosol  
832 products. *Rev. Geophys.*, 50, RG3005, doi:10.1029/2012RG000388, 2012.

833 Gobler C.J. and Sañudo-Wilhelmy S.A.: Effects of organic nitrogen, inorganic nutrients, and iron  
834 additions on the growth of phytoplankton and bacteria during a brown tide bloom. *Mar.*  
835 *Ecol. Prog. Ser.*, 209, 19-34, 2001.

836 Gonçalves Ageitos M., Obiso V., Miller R.L., Jorba O., Klose M., Dawson M., Balkanski Y., Perlwitz  
837 J., Basart S., Di Tomaso E., Escribano J., Macchia F., Montané G., Mahowald N., Green R.O.,  
838 Thompson D.R., Pérez García-Pando C.: Modeling dust mineralogical composition:  
839 sensitivity to soil mineralogy atlases and their expected climate impacts. *Atmos. Chem. and*  
840 *Phys* (Preprint), 1-51, <https://doi.org/10.5194/egusphere-2022-1414>.

841 González-Flórez C., Klose M., Alastuey A., Dupont S., Escribano J., Etyemezian V., Gonzalez-  
842 Romero A., Huang Y., Kandler K., Nikolich G., Panta A., Querol X., Reche C., Yus-Díez J., Pérez  
843 García-Pando C.: Insights into the size resolved dust emission from field measurements in  
844 the Moroccan Sahara. *Atmospheric Chemistry and Physics*, preprint, 2022.

845 [Gomes L.: Approche géochimique du soulèvement des aérosols à l'interface sol-atmosphère en](#)  
846 [zone désertique. Thesis Univ. Paris 7, 251 pp, 1990.](#)

847 Goudie A.S. & Middleton N.J.: *Desert dust in the global system*. Springer, Heidelberg. ISBN 978-  
848 3-540-32355-6, 288 pp, 2006.

849 Green R.O., Mahowald N., Ung C., Thompson D.R., Bator L., Bennet M., Zan J.: The earth surface  
850 mineral dust source investigation: an earth science imaging spectroscopy mission. In:  
851 *IEEE Aerospace Conference Proceedings*. IEEE Computer Society.  
852 <https://doi.org/10.1109/AERO47225.2020.9172731>. 2020.

853 [Grider, A., Ponette-González, A. and Heindel, R., 2023. Calcium and ammonium now control the](#)  
854 [pH of wet and bulk deposition in Ohio, US. \*Atmospheric Environment\*, 119986.](#)

855 Harrison A.D., Lever K., Sanchez-Marroquin A., Holden M.A., Whale T.F., Tarn M.D., McQuaid  
856 J.B., Murray B.J., The ice-nucleating ability of quartz immersed in water and its  
857 atmospheric importance compared to K-feldspar. *Atmos. Chem. Phys.*, 19, 11343–  
858 11361, 2019.

859 Horváth B., Opara-Nadi O., Beese F.: A simple method for measuring the carbonate content of  
860 soils. *SSSA*, 69 n° 4. 593-604, 2005.

861 Ito A. & Wagai R.: Global distribution of clay-size minerals on land surface for biogeochemical  
862 and climatological studies. *Scientific Data*, 4:170103, 2017. DOI: 10.1038/sdata.2017.103.

863 Journet E., Balkanski Y., Harrison S.P.: A new data set of soil mineralogy for dust-cycle modeling.  
864 *Atmos. Chem. Phys.*, 14, 8, 3801-3816, 2014.

865 Karanasiou A., Moreno N., Moreno T., Viana M., de Leeuw F., Querol X.: Health effects from  
866 Sahara dust episodes in Europe: Literature review and research gaps. *Environ. Int.* 47, 107–  
867 114, 2012.

868 Klose M., Jorba O., Gonçalves Ageitos M., Escribano J., Dawson M.L., Obiso V., Di Tomaso E.,  
869 Basart S., Montané Pinto G., Macchia F., Ginoux P., Guerschman J., Prigent C., Huang Y., Kok  
870 J.F., Miller R.L., and Pérez García-Pando C.: Mineral dust cycle in the Multiscale Online  
871 Nonhydrostatic Atmosphere Chemistry model (MONARCH) Version 2.0. *Geosci. Model*  
872 *Dev.*, 14, 6403–6444, <https://doi.org/10.5194/gmd-14-6403-2021>, 2021.

873 Kok J.F., Adebisi A.A., Albani S., Balkanski Y., Checa-Garcia R., Chin M., Colarco P.R., Hamilton  
874 D.S., Huang Y., Ito A., Klose M., Li L., Mahowald N.M., Miller R.L., Obiso V., Pérez García-  
875 Pando C., Rocha-Lima A., Wan J.S.: Contribution of the world's main dust source regions to  
876 the global cycle of desert dust. *Atmos. Chem. Phys.*, 21, 8169-8193, 2021.  
877 <https://doi.org/10.5194/acp-21-8169-2021>

878 Li L., Mahowald N., Miller R., Pérez García-Pando C., Klose M., Hamilton D., Gonçalves Ageitos  
879 M., Ginoux P., Balkanski Y., Green R., Kalashnikova O., Kok J., Obiso V., Paynter D., and  
880 Thompson D.: Quantifying the range of the dust direct radiative effect due to source

881 mineralogy uncertainty. *Atmospheric Chemistry and Physics*. 21, 3973–4005,  
882 <https://doi.org/10.5194/acp-21-3973-2021>, 2021.

883 [Mebius L.J.: A rapid method for the determination of organic carbon in soil. \*Analytica Chimica\*](#)  
884 [Acta, 22, 120-124, 1960.](#)

885 Middleton N.J.: Desert dust hazards: A global review. *Aeolian research*, 24, 53-63, 2017.

886 [Molinarioli E., Guerzoni S., Rampazzo G.: Contribution of Saharan dust to the central](#)  
887 [Mediterranean basin. \*Geological Society of America, Special paper\*, 284, 303-312, 1993.](#)

888 Monteiro A., Basart S., Kazadzia S., Votsis A., Gkikas A., Vandenbussche S., Tobias A., Gama C.,  
889 Pérez García-Pando C., Terradellas E., Notas G., Middleton N., Kushta J., Amiridis V.,  
890 Lagouvardos K., Kosmopoulos P., Kotroni V., Kanakidou M., Mihalopoulos N., Kalivitis N.,  
891 Dagsson-Waldhauserová P., El-Askary H., Sievers K., Giannaros T., Mona L., Hirtl M.,  
892 Skomorowski P., Virtanen T.H., Christoudias T., Di Mauro B., Tripetta S., Kutuzov S.,  
893 Meinander O., Nickovic S.: Multi-sectorial impact assessment of an extreme African dust  
894 episode in the Eastern Mediterranean in March 2018. *Science of the Total Environment*,  
895 843, 156861, 2022.

896 [Nelson D.W. & Sommers L.E.: A rapid and accurate method for estimating organic carbon in soil.](#)  
897 [Proceedings of the Indiana Academy of Science, 84, 456-462, 1975.](#)

898 Nickovic S., Vukovic A., Vujadinovic M., Djurdjevic V., Pejanovic G.: Technical Note: High-  
899 resolution mineralogical database of dust-productive soils for atmospheric dust modelling.  
900 *Atmos. Chem. Phys.*, 12, 2, 845-855, 2012.

901 Panta A., Kandler K., Alastuey A., González-Flórez C., González-Romero A., Klose M., Querol X.,  
902 Reche C., Yus-Díez J., Pérez García-Pando C.: Insights into the single particle composition,  
903 size, mixing state and aspect ratio of freshly emitted mineral dust from field measurements  
904 in the Moroccan Sahara using electron microscopy. *Atmospheric Chemistry and Physics*,  
905 preprint, 2022.

906 [Paulot, F., Ginoux, P., Cooke, W.F., Donner, L.J., Fan, S., Lin, M.Y., Mao, J., Naik, V. and Horowitz,](#)  
907 [L.W., 2016. Sensitivity of nitrate aerosols to ammonia emissions and to nitrate chemistry:](#)  
908 [implications for present and future nitrate optical depth. \*Atmospheric Chemistry and\*](#)  
909 [Physics, 16, 3, 1459-1477.](#)

910 Pérez C., Haustein K., Janjic Z., Jorba O., Huneus N., Baldasano J.M., Black T., Basart S., Nickovic  
911 S., Miller R.L., Perlwitz J. P., Schulz M., and Thomson M.: Atmospheric dust modeling from  
912 meso to global scales with the online NMMB/BSC-Dust model-Part 1: Model description,  
913 annual simulations and evaluation. *Atmos. Chem. Phys.*, 11, 13001–13027,  
914 <https://doi.org/10.5194/acp-11-13001-2011>, 2011.

915 Pérez García-Pando C., Stanton M.C., Diggle P.J., Trzaska S., Miller R.L., Perlwitz J.P., Baldasano  
916 J.M., Cuevas E., Ceccato P., Yaka P., Thomson M.C.: Soil dust aerosols and wind as predictors  
917 of seasonal meningitis incidence in Niger. *Environ. Health Perspect.* 122, 7679-686, 2014.

918 Perlwitz J.P., Pérez García-Pando C., and Miller R.L.: Predicting the mineral composition of dust  
919 aerosols – Part 1: Representing key processes. *Atmos. Chem. Phys.* 15, 11593–11627,  
920 <https://doi.org/10.5194/acp-15-11593-2015>, 2015.

921 Prospero J.M., Ginoux P., Torres O., Nicholson S.E., Gill T.E.: Environmental characterization of  
922 global sources of atmospheric soil dust identified with the Nimbus 7 Total Ozone Mapping  
923 Spectrometer (TOMS) absorbing aerosol product. *Rev. Geophys.*, 40, 1, 1002,  
924 doi:10.1029/2000RG000095, 2002.

925 Pye K. & Tsoar H.: The mechanics and geological implications of dust transport and deposition  
926 in deserts with particular reference to loess formation and dune sand diagenesis in the  
927 northern Negev, Israel. *Geol. Soc. Of London Publ.* 139-156, doi:  
928 10.1144/GSL.SP.1987.035.01.10, 2015.

929 Querol X.: The Occurrence and Distribution of Trace Elements in the Teruel Mining District Coals  
930 and their Behaviour during Coal Combustion. European Coal and Steel Community Project  
931 7220/ED/014, 1993.

932 Querol X., Whateley M.K.G., Fernandez-Turiel J.L., Tuncali E.: Geological controls on the  
 933 mineralogy and geochemistry of the Beypazari lignite, Central Anatolia, Turkey. *Int. J. Coal.*  
 934 *Geol.*, 33:255–271, 1997.

935 Querol X., Tobías A., Pérez N., Karanasiou A., Amato F., Stafoggia M., Pérez García-Pando C.,  
 936 Ginoux P., Forastiere F., Gumy S., Mudu P., Alastuey A.: Monitoring the impact of desert  
 937 dust outbreaks for air quality for health studies. *Env. International*, 130, 104867, 2019.

938 Reynolds R.L., Cattle S.R., Moskowit B.M., Goldstein H.L., Yauk K., Flagg C.B., Berquó T.S., Kokaly  
 939 R.F., Morman S., Breit G.N. : Iron oxide minerals in dust of the Red Dawn event in eastern  
 940 Australia, September 2009. *Aeolian Research*, 15, 1-13, 2014.

941 [Sabre M.: Étude dynamique du processus d'Émission de poussières désertiques: impact sur le](#)  
 942 [fractionnement chimique entre sol et aérosol. Thesis Univ. Paris 7, 170 pp, 1997.](#)

943 Scanza R.A., Mahowald N., Ghan S., Zender C.S., Kok J.F., Liu X., Zhang Y., Albani S.: Modelling  
 944 dust as component minerals in the Community Atmosphere Model: development of  
 945 framework and impact on radiative forcing. *Atmos. Chem. Phys.*, 15, 537–561, 2015.

946 Scheuvs D., Schütz L., Kandler K., Ebert M., Weinbruch S.: Bulk composition of northern  
 947 African dust and its source sediments - A compilation. *Earth-Science Rev.*, 116, 1, 170-194,  
 948 2013.

949 [Schütz L. & Seibert M.: Mineral aerosols and source identification. \*Journal of Aerosol Science\* 18,](#)  
 950 [1, 1-10, 1987.](#)

951 Shao Y., Ishizuka M., Mikami M., Leys J.F.: Parameterization of size-resolved dust emission and  
 952 validation with measurements. *J. Geophys. Res.*, 116, D08203. doi:10.1029/2010JD014527,  
 953 2011.

954 Shen Z., Caquineau S., Cao J., Zhang X., Hana Y., Gaudichet A., Gomes L.: Mineralogical  
 955 characteristics of soil dust from source regions in northern China. *Particology* 7, 507-512,  
 956 2009.

957 Shi Z.B., Krom M.D., Bonneville S.: Formation of Iron Nanoparticles and Increase in Iron  
 958 Reactivity in Mineral Dust during Simulated Cloud Processing. *Environ. Sci. Technol.* 43,  
 959 6592-6596, 2009.

960 Shi Z.B., Krom M.D., Jickells T.D., Bonneville S., Carslaw K. S., Mihalopoulos N., Baker A. R.,  
 961 Benning L. G.: Impacts on iron solubility in the mineral dust by processes in the source  
 962 region and the atmosphere: A review. *Aeolian Research*, 5, 21-42.  
 963 <https://doi.org/10.1016/j.aeolia.2012.03.001>, 2012.

964 Sokolik I.N. & Toon O.B.: Incorporation of mineralogical composition into models of the radiative  
 965 properties of mineral aerosol from UV to IR wavelengths. *J. Geophys. Res.*, 104, 9423-9444,  
 966 1999.

967 Sperazza M., Moore J.N., Hendrix M.: High-Resolution particle size analysis of naturally occurring  
 968 very fine-grained sediment through laser diffractometry. *J. Sediment. Res.*, 74(5):736-743,  
 969 2004.

970 Stout J.E., Lee J.A.: Indirect evidence of wind erosion trends on the Southern High Plains of North  
 971 America. *Journal of Arid Environments*, 55, 1, 43-61, 2003.

972 [Subramaniam N., Al-Sudairawi M., Al-Dousari A., Al-Dousari N.: Probability distribution and](#)  
 973 [extreme value analysis of total suspended particulate matter in Kuwait. \*Arab. J. Geosci.\*, 8,](#)  
 974 [11329-11344, 2015. <https://doi.org/10.1007/s12517-015-2008-z>](#)

975 Sullivan R.C., Guazzotti S.A., Sodeman D.A., Tang Y., Carmichael G.R., Prather K.A.: Mineral dust  
 976 is a sink for chlorine in the marine boundary layer. *Atmos. Environ.* 41, 7166-7179, 2007.

977 Tegen I., Harrison S.P., Kohfeld K., Prentice I.C., Coe M., Heimann M.: Impact of vegetation and  
 978 preferential source areas on global dust aerosol: Results from a model study. *Journal of*  
 979 *Geophysical Research: Atmospheres*, 107, D21, AAC 14-a-AAC 14-27, 2002.

980 [Tegen I., Hollrig P., Chin m., Fung I., Jacob D., Penner J.: Contribution of different aerosol](#)  
 981 [extinction optical thickness: Estimates from model results. \*Journal of Geophysical Research:\*](#)  
 982 [Atmospheres, 102, D21, 23895-23915, 1997.](#)

Con formato: Inglés (Reino Unido)

983 Tegen I., Fung I.: Modeling of mineral dust in the atmosphere: Sources, transport, and optical  
984 thickness, *J. Geophys. Res.*, **99**, 22897-22914, 1994.

985 Thorez, J.: Practical Identification of clay minerals. G. Lellote, Dison (Belgique), 90pp, 1976.

986 Urquhart L. C.: *Civil Engineering Handbook*, McGraw Hill, New York, 1959

987 Valentin C. & Bresson L.M.: Morphology, génesis and classification of Surface crusts in loamy  
988 and Sandy soils. *Geoderma*, **55**, 225-245, 1992.

989 Van der Watt H.v.H. & Valentin C.: Soil crusting: The African view. In Summer, M.E., Stewart, B.A.  
990 (Eds.), *Soil Crusting, Chemical and Physical Processes*. CRC Press, Boca Raton, 301-338,  
991 1992.

992 Walkley A. & Black I.A.: An examination of Degtjareff method for determining soil organic matter  
993 and a proposed modification of the chromic acid titration method. *Soil Science*, **37**, 29-37,  
994 1934.

995 Weaver C.J., Ginoux P., Hsu N.C., Chou M.-D., Joiner J.: Radiative forcing of Saharan dust:  
996 GOCART model simulations compared with ERBE data. *J. Atmos. Sci.*, **59**:736-747, 2002.

997 Wentworth C.K.: A scale of grade and class terms for clastic sediments. *The journal of geology*,  
998 **30**, 5, 377-392, doi:10.1086/622910, 1922.

999 Yus-Díez J., Pandolfi M., González-Flórez C., Escibano J., Gonzalez-Romero A., Ivancic M., Rigler  
1000 M., Klose M., Kandler K., Panta A., Querol X., Reche C., Pérez García-Pando C., and Alastuey,  
1001 A.: Quantifying variations in multi-wavelength optical properties of freshly-emitted Saharan  
1002 dust from the Lower Drâa Valley, Moroccan Sahara, in prep

1003 Zender C.S., Newman D., Torres O.: Spatial heterogeneity in aeolian erodibility: Uniform,  
1004 topographic, geomorphic, and hydrologic hypotheses. *Journal of Geophysical Research-*  
1005 *Atmospheres* **108**, 4543, 2003.

1006 Zender C.S., Miller R.L., Tegen I.: Quantifying mineral dust mass budgets: Terminology,  
1007 constraints, and current estimates. *Eos, Transactions American Geophysical Union*. **85**, 48,  
1008 509-512, <https://doi.org/10.1029/2004EO480002>, 2004

1009  
1010  
1011  
1012  
1013  
1014  
1015  
1016  
1017  
1018  
1019  
1020  
1021  
1022  
1023  
1024



1025 **Figure captions**

1026 **Figure 1.** a) Location of the study area (exact location of data measurement “star”: 29°49’30”N,  
1027 5°52’25”W), near M’Hamid el Ghizlane, into the Drâa basin in S Morocco. Base layer from  
1028 world imagery of Google Earth Pro v:7.3.6.9345. b) Frequency of occurrence (%) of dust  
1029 optical depth above 0.2 in September, October and November between 2003 and 2016  
1030 derived from MODIS Deep Blue. c) EMIT scenes  
1031 emit20220903t082303\_o24606\_s001\_l2a\_rfl\_b0106\_v01 and  
1032 emit20230206t101334\_o03707\_s000\_l2a\_rfl\_b0106\_v01 at 60 meters per pixel show the  
1033 diversity of Fe<sup>2+</sup> and Fe<sup>3+</sup> bearing minerals (left) and the EMIT 8 phyllosilicates, carbonates,  
1034 and sulphates (right). The mineral maps were produced by tetracorder 5.27c1 (Clark, 2023).  
1035 There is some mapped mineralogy difference at the scene boundaries, possibly due to the  
1036 changing viewing geometry, and variation in atmospheric removal between the two scenes.  
1037 Cirrus clouds in the scene on the right may also be impacting derived mineralogy.

1038 **Figure 2.** Images of samples collected during a field campaign near M’Hamid el Ghizlane, into  
1039 the Draa Basin, S Morocco.

1040 **Figure 3.** Median minimally and fully dispersed PSDs of crusts, sediments, paved sediments and  
1041 dunes. (a) MDPSDs and (b) FDPDSs combined from crust, sediment and paved sediment  
1042 samples; (c) and (d) are MDPSDs and FDPDSs for dune samples; (e) and (f) are MDPSDs and  
1043 FDPDSs differentiated by type of sample.

1044 **Figure 4.** Boxplot of median ~~particle-size~~ particle-size diameters in µm including both fully and  
1045 minimally dispersed analysis (a) for all samples combined excluding dunes and (b) for dune  
1046 samples only. Also ~~particle-size~~ particle-size diameter in µm for crusts, sediment and paved  
1047 sediment for (c) minimally dispersed and (d) fully dispersed results. Means median  
1048 diameters for each sediment type are shown with crosses.

1049 **Figure 5.** Spatial variation map with crust fully dispersed mean median particle diameter.

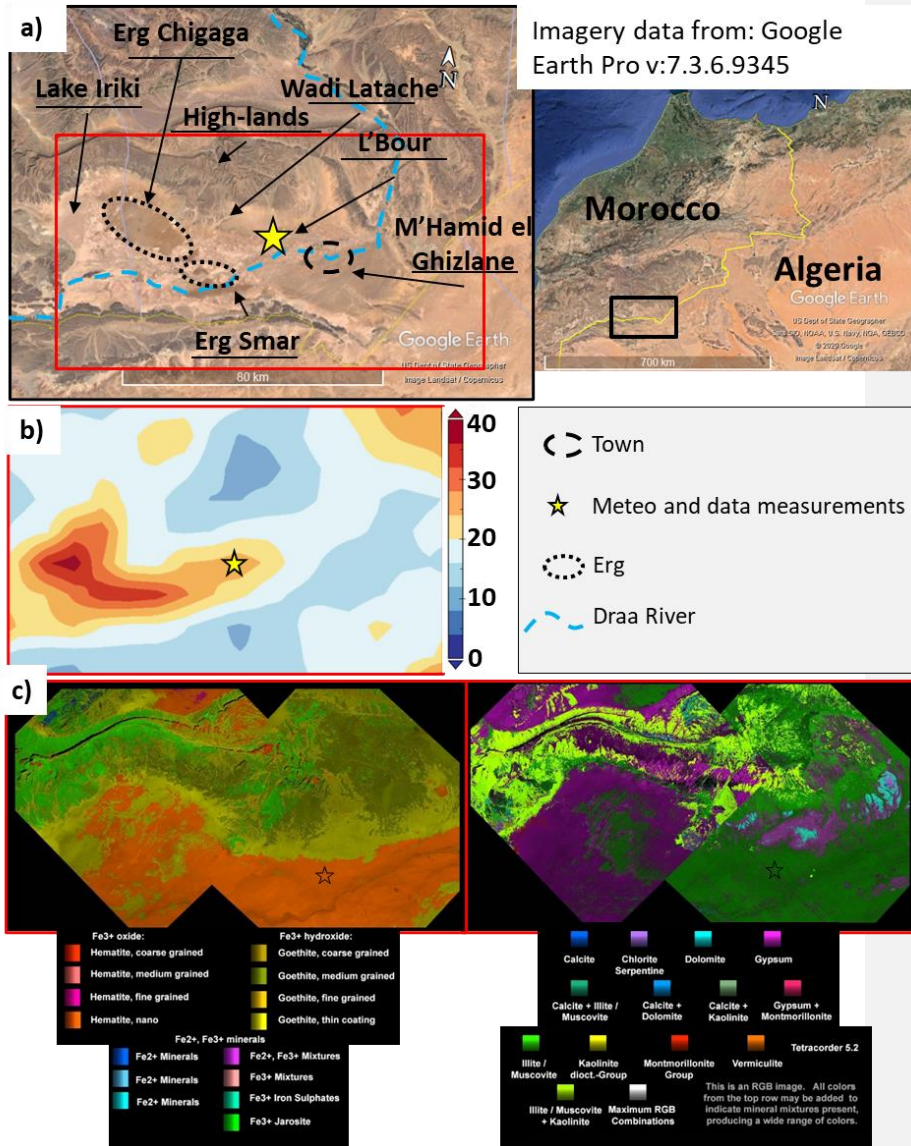
1050 **Figure 6.** Mean mineral group content of dune, crust, paved sediment and sediment samples,  
1051 and also at Erg Smar, L’Bour and High-lands. Solid lines mark the mean content of all the  
1052 samples (excluding dune samples). The dashed line divides between type and location of  
1053 the samples.

1054 **Figure 7.** Schematic model of sedimentation and deposition processes in ~~our~~ the study site from  
1055 high-lands to low-lands for a) crusts and for b) paved sediments.

1056 **Figure 8.** Dust emission conceptual model integrating ~~particle-size~~ particle-size distributions and  
1057 mineralogy of dust ~~source-hotspots~~ source-hotspots sediments. a) Refers to the conceptual thickness and  
1058 ~~particle-size~~ particle-size distributions along the basin, b) to the ~~particle-size~~ particle-size  
1059 distribution and segregation of mineralogy and c) to the dust emission quantity expected  
1060 depending on the place in the basin.

1061  
1062  
1063





1064  
 1065  
 1066  
 1067  
 1068  
 1069  
 1070

Figure 1.

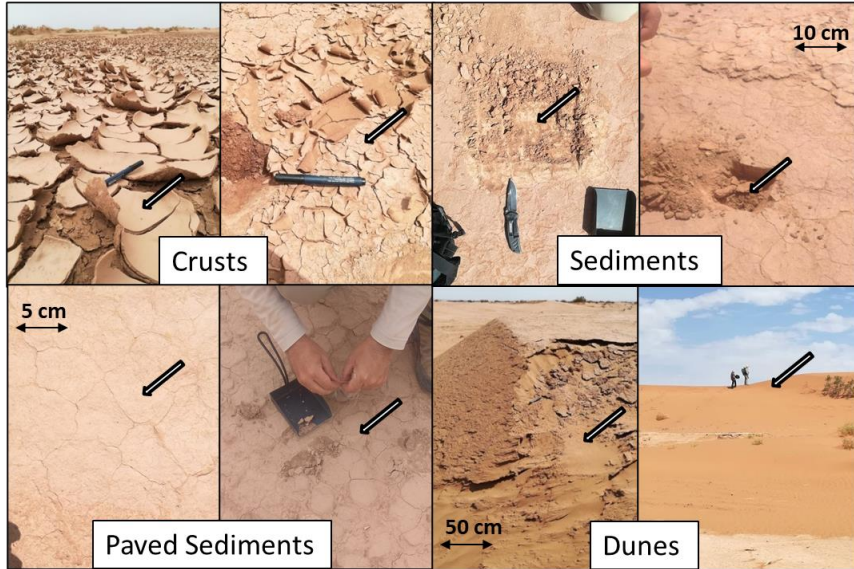
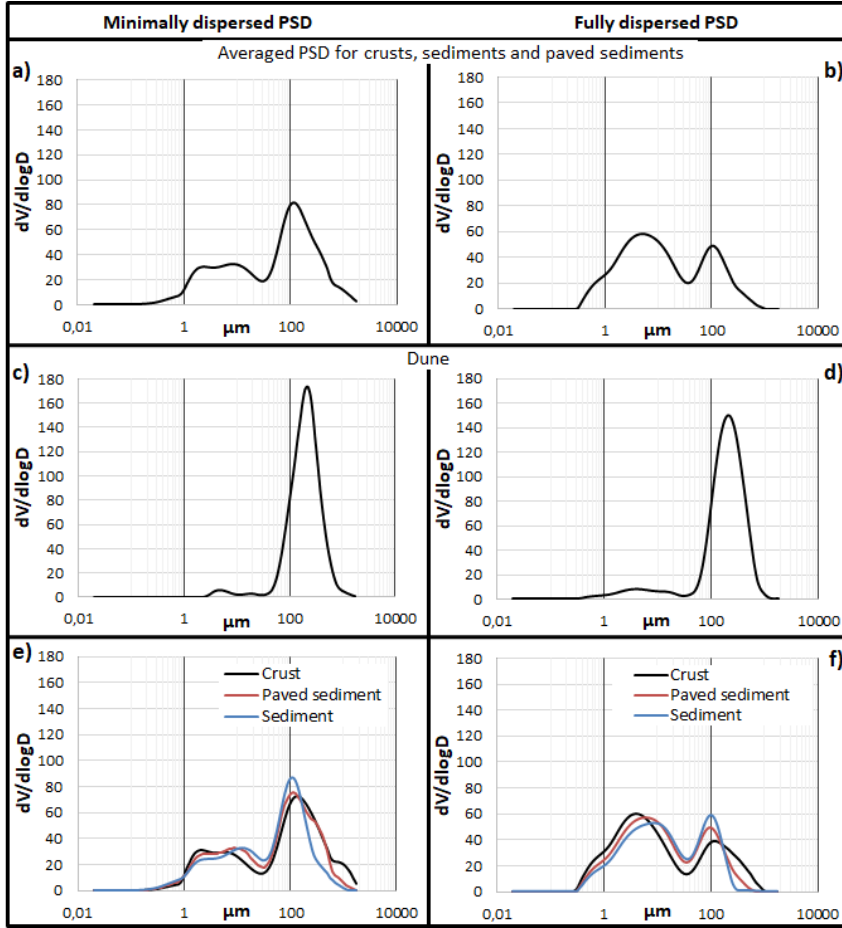


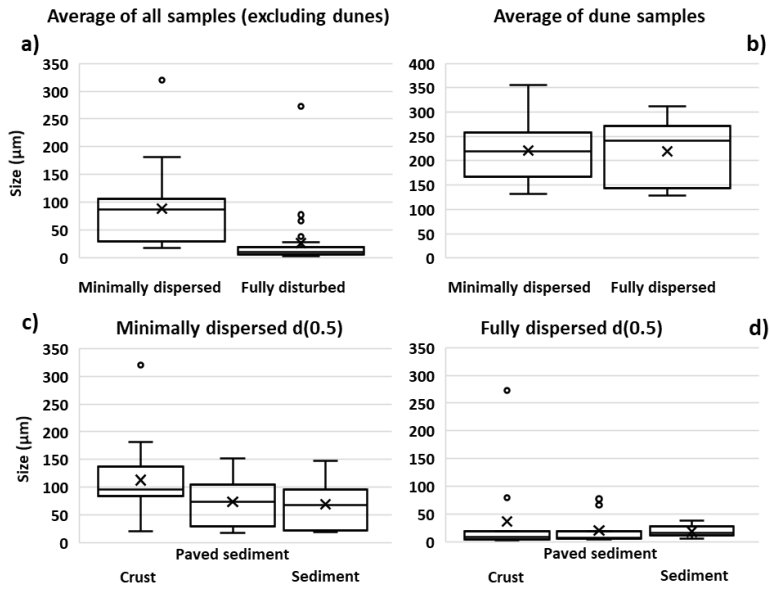
Figure 2.

1071  
 1072  
 1073  
 1074  
 1075  
 1076  
 1077  
 1078  
 1079  
 1080  
 1081  
 1082  
 1083  
 1084  
 1085  
 1086  
 1087  
 1088  
 1089  
 1090  
 1091  
 1092  
 1093  
 1094  
 1095  
 1096  
 1097  
 1098

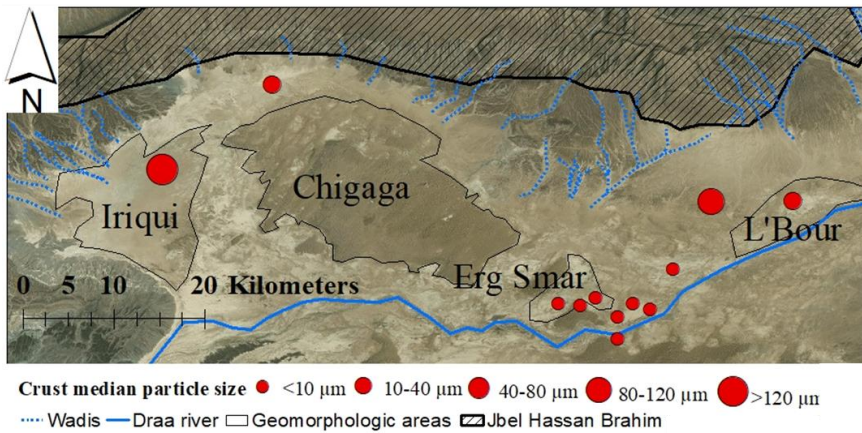


1099  
 1100  
 1101  
 1102  
 1103  
 1104  
 1105  
 1106  
 1107  
 1108  
 1109  
 1110  
 1111  
 1112

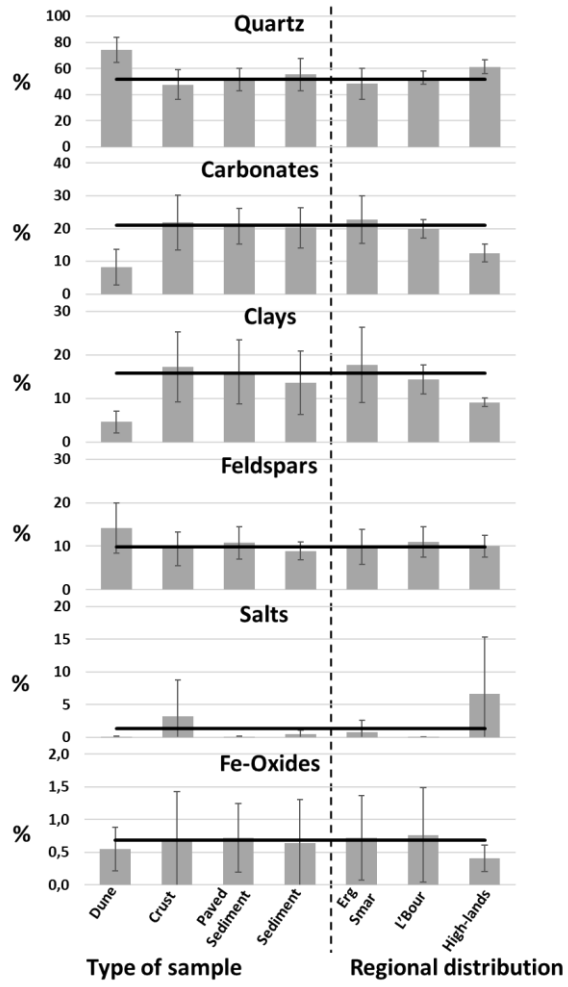
Figure 3.



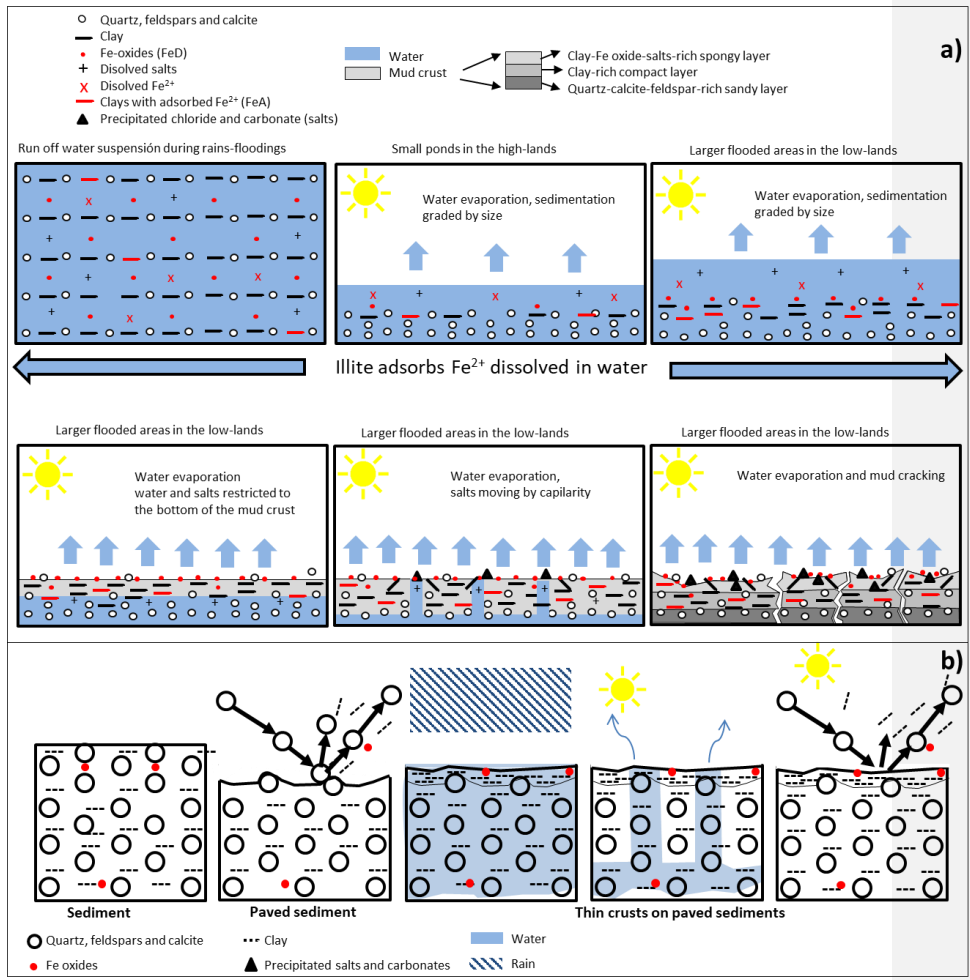
1113  
 1114  
 1115  
 1116  
 1117  
 Figure 4.



1118  
 1119  
 1120  
 1121  
 1122  
 Figure 5.



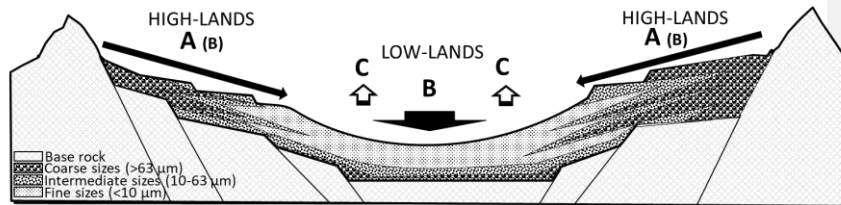
1123  
 1124 Figure 6.  
 1125  
 1126  
 1127  
 1128  
 1129  
 1130  
 1131  
 1132  
 1133



1134  
 1135  
 1136  
 1137  
 1138  
 1139  
 1140  
 1141  
 1142  
 1143  
 1144  
 1145  
 1146  
 1147  
 1148  
 1149

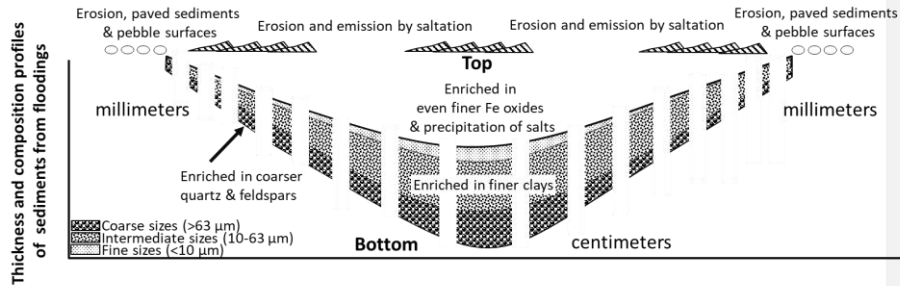
Figure 7.

**a. Macro-scale (basin) size and mineral segregation of sediments**

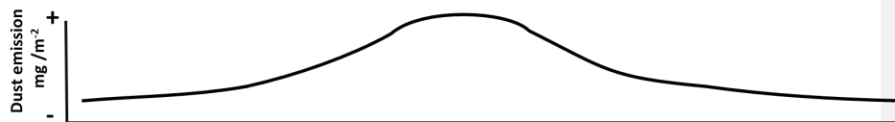


A: Washout, erosion and sporadic flooding with deposition of coarser sediments enriched in quartz and feldspars  
 B: Flooding and deposition of finer sediments enriched in clays and Fe oxides  
 C: Evaporation and deposition of fine clays and readily exchangeable Fe oxide, salt crystallization in upper layers

**b. Micro-scale (profiles of deposited sediments) size and mineral segregation**



**c. Higher dust emissions (high Fe oxide and clay) in low-lands with thicker & finer deposited sediments**



**a+b+c= Emitted dust might be markedly enriched in clays and Fe oxides compared to the parent sediments/soils**

1150  
 1151  
 1152  
 1153  
 1154  
 1155  
 1156  
 1157

Figure 8.



Table 1. Full range, <63µm and >63 to 2000 µm mean diameter, standard deviation, min., max. and for Minimally dispersed particle size distribution and fully dispersed particle size distribution.

Surface Type	Location	N° of samples	MDPSD		
			Full range	≤ 63 µm	>63 to 2000 µm
Mean of medians ± sd [Min,Max]					
Dunes	Mean	12	221 ± 64 [132,355]	32 ± 9.3 [20,46]	252 ± 65 [142,364]
	High-Land	3	212 ± 27 [195,243]	45 ± 1.3 [44,46]	259 ± 22 [243,284]
	Erg Smar	4	286 ± 49 [244,355]	32 ± 8.1 [25,41]	295 ± 52 [238,364]
	L'Bour	5	174 ± 45 [132,244]	27 ± 7.4 [20,36]	214 ± 76 [142,332]
Crusts	Mean	12	113 ± 79 [20, 320]	15 ± 3.7 [7.7,19]	308 ± 146 [146,635]
	High-Land	3	94 ± 5 [89,99]	18 ± 1.1 [17,19]	219 ± 28 [187,238]
	Erg Smar	8	131 ± 89 [21,320]	13 ± 3.4 [7.7,17]	362 ± 151 [193,635]
	L'Bour	1	20 ± NA [NA,NA]	15 ± NA [NA,NA]	146 ± NA [NA,NA]
Paved Sediments	Mean	11	74 ± 48 [19,152]	17 ± 6.7 [11,33]	237 ± 71 [146,387]
	High-Land	0	NA	NA	NA
	Erg Smar	8	68 ± 46 [19, 148]	17 ± 7.0 [11,33]	240 ± 43 [167,320]
	L'Bour	3	90 ± 61 [29,148]	18 ± 7.1 [13,26]	230 ± 137 [146,387]
Sediments	Mean	7	70 ± 45 [20,147]	18 ± 5.1 [15,29]	175 ± 58 [129,302]
	High-Land	1	97 ± NA [NA,NA]	18 ± NA [NA,NA]	149 ± NA [NA,NA]
	Erg Smar	2	115 ± 45 [83,147]	22 ± 11 [15,29]	229 ± 104 [155,302]
	L'Bour	4	40 ± 23 [20,68]	17 ± 0.79 [16,17]	155 ± 21 [129,178]
FDPSD					
Dunes	Mean	12	219 ± 70 [128,312]	24 ± 13 [9.0,46]	247 ± 72 [145,355]
	High-Land	3	250 ± 73 [169,312]	41 ± 6.8 [33,46]	290 ± 77 [205,355]
	Erg Smar	4	263 ± 32 [239,308]	20 ± 6.2 [13,25]	279 ± 33 [238,319]
	L'Bour	5	166 ± 61 [128,272]	16 ± 7.5 [9.0,26]	195 ± 68 [145,310]
Crusts	Mean	12	37 ± 77 [2.7,272]	9.8 ± 3.6 [3.6,16]	196 ± 76 [119,389]
	High-Land	3	124 ± 132 [20,272]	13 ± 1.1 [12,14]	251 ± 121 [162,389]
	Erg Smar	8	7 ± 3 [2.7,10]	7.9 ± 2.5 [3.6,11]	183 ± 44 [130,236]
	L'Bour	1	17 ± NA [NA,NA]	16 ± NA [NA,NA]	119 ± NA [NA,NA]
Paved Sediments	Mean	11	21 ± 26 [2.3,78]	13 ± 4.8 [8.2,21]	157 ± 36 [120,221]
	High-Land	0	NA	NA	NA
	Erg Smar	8	18 ± 24 [5.9,78]	12 ± 4.6 [8.2,21]	169 ± 34 [129,221]
	L'Bour	3	29 ± 33 [5.3,67]	14 ± 6.0 [8.3,20]	122 ± 2.2 [120,124]
Sediments	Mean	7	19 ± 11 [5.8,39]	14 ± 3.9 [7.7,19]	128 ± 9.6 [117,144]
	High-Land	1	12 ± NA [NA,NA]	9.9 ± NA [NA,NA]	133 ± NA [NA,NA]
	Erg Smar	2	22 ± 23 [5.8,39]	13 ± 8.1 [7.7,19]	126 ± 13 [117,135]
	L'Bour	4	19 ± 6.3 [13,28]	15 ± 1.3 [13,17]	128 ± 11 [122,144]



Table 2. Mineral results from samples and type of sample. In type of samples, C: Crust, PS: Paved sediment, S: Sediment, D: Dune. In Loc (Location), ES: Erg Smar, LB: L'Bour, HL: High-lands. Sme: Smectite, Mca: Mica/Illite, Kln: Kaolinite, Chl: Chlorite, Plg: Palygorskite, Qtz: Quartz, Cal: Calcite, Dol: Dolomite, Hl: Halite, Gp: Gypsum, Mc: Microcline, Ab: Albite and anorthite, Hem: Hematite, Gt: Goethite. <0.1 indicates below limit of detection.

Type	LOC	Qtz	Feldspars		Carbonates		Clays				Salts		Iron Oxides		
			Mc	Ab	Cal	Dol	Sme	Mca	Kln	Chl	Plg	Hl	Gp	Hem	Gt
C	ES	55	2,6	4,8	20	3,3	<0.1	11	<0.1	1,2	<0.1	<0.1	<0.1	1,2	<0.1
C	ES	57	2,7	3,1	20	3,4	<0.1	5,2	<0.1	0,78	0,26	7,2	<0.1	0,87	<0.1
C	ES	36	2,2	10	21	2,7	<0.1	15	10,0	1,4	<0.1	<0.1	0,20	1,2	<0.1
C	ES	32	1,7	3,3	29	3,4	<0.1	10	17	2,2	0,20	<0.1	<0.1	0,24	1,3
C	ES	38	3,7	4,7	18	6,2	<0.1	14	9,0	1,3	0,14	3,5	0,14	0,95	<0.1
C	ES	50	5,5	5,5	14	2,8	<0.1	12	7,9	1,3	<0.1	<0.1	<0.1	0,21	0,85
C	LB	50	13	5,1	12	3,6	<0.1	8,1	5,7	0,46	<0.1	<0.1	<0.1	0,92	<0.1
C	HL	63	6,9	6,8	12	2,2	<0.1	4,5	3,9	0,19	<0.1	<0.1	<0.1	0,11	0,40
C	ES	45	3,7	3,2	26	3,2	<0.1	11	5,4	1,8	0,21	<0.1	<0.1	<0.1	0,18
C	ES	30	2,6	3,4	35	2,5	0,57	8,8	14	1,4	1,5	0,14	<0.1	0,14	0,17
C	HL	60	3,7	5,5	11	0,98	<0.1	5,7	3,4	0,97	0,19	8,1	0,21	0,41	0,60
C	HL	54	4,7	3,9	7,1	1,79	<0.1	5,4	3,3	0,60	<0.1	16	2,0	0,22	0,65
S	ES	35	1,8	4,1	24	5,6	<0.1	17	8,3	2,2	<0.1	1,1	0,19	1,1	<0.1
S	ES	67	6,6	5,1	10	2,1	<0.1	3,0	3,6	0,64	<0.1	1,1	<0.1	0,42	0,23
S	LB	51	4,6	7,9	15	4,2	<0.1	8,9	6,6	0,89	<0.1	<0.1	<0.1	<0.1	0,82
S	LB	57	2,7	7,8	16	3,8	<0.1	9,6	1,9	0,49	<0.1	<0.1	<0.1	0,93	<0.1
S	LB	57	3,4	5,4	18	3,2	<0.1	6,5	3,5	2,1	<0.1	<0.1	<0.1	0,33	0,60
S	HL	67	3,2	5,3	13	1,7	0,13	4,3	3,2	0,20	0,20	<0.1	<0.1	<0.1	0,90
S	LB	51	3,4	5,1	21	3,3	<0.1	8,5	4,5	2,2	0,15	<0.1	<0.1	0,66	0,50
PS	ES	44	3,0	5,7	15	3,1	<0.1	16	11	1,5	<0.1	<0.1	<0.1	0,35	0,64
PS	ES	44	2,2	5,4	22	4,7	<0.1	13	6,8	0,54	<0.1	<0.1	<0.1	1,1	<0.1
PS	ES	55	2,3	5,4	24	3,6	<0.1	7,8	0,84	0,28	0,17	<0.1	<0.1	0,98	<0.1
PS	ES	40	5,3	4,7	20	4,3	<0.1	13	10	1,1	<0.1	<0.1	0,29	0,77	0,23
PS	ES	67	8,8	8,7	8,9	1,8	<0.1	3,1	0,38	0,30	<0.1	<0.1	<0.1	0,30	0,29
PS	LB	48	5,5	4,0	16	4,3	<0.1	11	8,7	1,3	0,13	<0.1	<0.1	1,1	<0.1
PS	ES	61	3,5	6,3	12	3,6	<0.1	7,9	3,6	0,78	0,16	<0.1	<0.1	0,41	0,33
PS	ES	46	9,1	9,0	14	3,3	0,29	6,6	8,8	1,0	0,42	<0.1	<0.1	0,42	0,69
PS	ES	48	2,3	7,3	22	3,7	<0.1	8,1	6,3	1,3	<0.1	<0.1	0,16	0,17	1,1
PS	LB	61	4,0	8,1	13	3,3	<0.1	4,3	4,2	1,2	<0.1	<0.1	<0.1	0,16	0,64
PS	LB	51	3,6	4,4	22	3,1	<0.1	8,5	4,3	2,0	0,17	<0.1	<0.1	0,68	0,53
D	ES	80	7,1	7,0	3,1	0,69	<0.1	1,4	<0.1	<0.1	<0.1	<0.1	<0.1	<0.1	0,38
D	ES	65	14	8,3	4,1	0,90	<0.1	4,8	1,9	<0.1	<0.1	<0.1	<0.1	<0.1	0,37
D	LB	73	7,0	11	6,6	0,31	<0.1	1,2	0,19	0,23	<0.1	<0.1	<0.1	0,11	0,32
D	ES	89	2,5	3,0	2,0	<0.1	<0.1	0,69	1,4	<0.1	<0.1	<0.1	<0.1	0,45	0,65
D	ES	65	12	5,4	11	1,3	0,13	2,7	2,1	0,38	<0.1	<0.1	<0.1	0,12	0,32
D	LB	64	5,0	6,8	10	5,0	<0.1	3,1	4,3	0,50	<0.1	<0.1	<0.1	<0.1	0,61
D	LB	76	4,1	6,7	6,6	0,52	<0.1	2,6	2,2	0,21	<0.1	0,28	<0.1	0,25	0,21
D	LB	77	3,9	6,7	7,5	0,53	0,26	1,5	1,6	0,49	<0.1	0,34	<0.1	0,13	0,50
D	LB	57	11	14	7,5	1,8	<0.1	3,4	3,0	0,74	<0.1	<0.1	<0.1	0,16	0,37
D	HL	85	4,8	4,0	3,7	0,33	<0.1	1,1	0,22	0,51	<0.1	<0.1	<0.1	<0.1	0,69
D	HL	82	9,2	3,3	2,8	0,17	0,15	1,2	0,67	<0.1	<0.1	<0.1	<0.1	0,20	0,29
D	HL	77	6,9	7,3	4,5	0,34	<0.1	1,7	1,3	0,39	<0.1	<0.1	<0.1	<0.1	0,41

Table 3. Mineralogy of specific soils according to Claquin et al. (1999) and Journet et al. (2014) and comparison with the one obtained in this study for six selected samples. Bulk, clay and silt fractions mineralogy (obtained from texture fractionation) and <10 µm and silt (10-63 µm) fractions mineralogy using fully dispersed separation. All content is in mass %.

	Carbonates				Clays					Salts		Fe-oxides		
	Qtz	Feld	Cal	Dol	Mca	Chl	Sme	Plg	Kln	Tot.clay	Gp	Hal	Hem	Gt
Bulk	58	9.5	15	2.4	6.4	1.0	0.1	0.2	3.8	11	0.2	8.1	0.5	0.5
Clay Ye Claquin	5	NA	6	NA	89	NA	NA	NA	NA	≈89	NA	NA	NA	NA
Clay Ye Journet	8	3	18	NA	67	NA	NA	1	3	≈71	NA	NA	NA	NA
Clay Fl Claquin	12	NA	11	NA	77	NA	NA	NA	NA	≈77	NA	NA	NA	NA
Clay Fl Journet	NA	NA	NA	NA	98	NA	NA	1	1	≈100	NA	NA	NA	NA
Clay classic Drâa	17	7.1	8.9	0.5	23	9.9	1.2	1.0	22	57	NA	NA	0.7	5.2
<10µm FD Drâa	23	4.7	19	2.4	19	4.7	0.4	0.2	14	38	NA	NA	2.2	1.8
Silt Ye Claquin	58	31	8	NA	NA	NA	NA	NA	NA	NA	2	NA	1	NA
Silt Ye Journet	43	21	20	NA	9	6	NA	NA	NA	15	NA	NA	1	NA
Silt Fl Claquin	30	38	29	NA	NA	NA	NA	NA	NA	NA	2	NA	NA	NA
Silt Fl Journet	39	19	12	NA	19	10	NA	NA	NA	29	NA	NA	1	NA
Silt classic Drâa	30	8	12	4.9	19	6.4	0.3	0.1	13	39	NA	NA	0.2	0.6
Silt FD Drâa	39	8.0	23	5.0	12	2.8	0.2	<0.1	7.5	23	NA	NA	1.2	0.7

Fl: Fluvisol sediment type; Ye: Yermosol; Qtz: Quartz; Feld: Feldspars; Cal: Calcite; Dol: Dolomite; Mca: Mica/illite; Chl: Chlorite; Sme: Smectite; Plg: Palygorskite; Kln: Kaolinite; Gp: Gypsum; Hal: Halite; Hem: Hematite; Gt: Goethite; FD: fully dispersed.



